0 0 0 4 8 0 0 9 2 1

uc-34d

LBL-6438 c.1

HADRONIC STRUCTURE OF THE WEAK NEUTRAL CURRENT

John Marriner
(Ph. D. thesis)

RECEIVED
LAWRENCE
BERKELEY LABORATORY
NOV 16 1977
DOCUMENTS SECTION

September 1977

Prepared for the U. S. Energy Research and
Development Administration under Contract W-7405-ENG-48

For Reference

Not to be taken from this room

LAWRENCE BERKELEY LABORATORY
UNIVERSITY OF CALIFORNIA
BERKELEY

LBL-6438 c.1

DISCLAIMER

This document was prepared as an account of work sponsored by the United States Government. While this document is believed to contain correct information, neither the United States Government nor any agency thereof, nor the Regents of the University of California, nor any of their employees, makes any warranty, express or implied, or assumes any legal responsibility for the accuracy, completeness, or usefulness of any information, apparatus, product, or process disclosed, or represents that its use would not infringe privately owned rights. Reference herein to any specific commercial product, process, or service by its trade name, trademark, manufacturer, or otherwise, does not necessarily constitute or imply its endorsement, recommendation, or favoring by the United States Government or any agency thereof, or the Regents of the University of California. The views and opinions of authors expressed herein do not necessarily state or reflect those of the United States Government or any agency thereof or the Regents of the University of California.

0 0 0 0 4 8 0 1 9 2 2

HADRONIC STRUCTURE OF THE WEAK NEUTRAL CURRENT

John Marriner

Lawrence Berkeley Laboratory
University of California
Berkeley, California 94720

ABSTRACT

A comparison of neutral and charged current deep inelastic neutrino interactions is made in an experiment utilizing the Fermilab 15 ft. bubble chamber. The ratio of neutral current events (NC) to charged current events (CC) is 0.35 ± .06 when the visible hadronic energy is greater than 10 GeV. The distributions of NC and CC in a new variable called u_{vis}, which depends only on the observed hadrons, are given. From these distributions and the assumption that the x distribution is the same for NC and CC, it is concluded that for a NC y distribution of the form $(1-\eta) + 3\eta(1-y)^2$, $\eta = .12 \pm .32$. The ratio $\rho_{NC}(\rho_{CC})$ of neutron to proton cross sections in NC (CC) is studied and the quotient $\rho_{NC}/\rho_{CC} = 0.7 \pm 0.2$. The distribution of hadrons in z_{vis}, the scaled hadronic momentum, is given. The CC hadrons fit the predictions of the quark fragmentation functions $D_u^{\pi^+}(z)$ and $D_u^{\pi^-}(z)$ as given by Field and Feynman. The neutral current events fit the form $(1-\lambda)\, D_u^{\pi^+}(z) + \lambda\, D_d^{\pi^+}(z)$ for positives and $(1-\lambda)\, D_u^{\pi^-}(z) + \lambda\, D_d^{\pi^-}(z)$ for negatives with $\lambda = 0.56 \pm 0.10$ and a fit confidence level of 4%.

CONTENTS

I. INTRODUCTION. A qualitative overview of the weak neutral current and lepton nucleon scattering is given. 1

II. THEORETICAL DESCRIPTION-QUARK PARTON MODEL. The relevant results of the quark parton model are summarized. 4

III. EXPERIMENT ARRANGEMENT. The distinctive features of the experimental apparatus are described. . . . 12

IV. ANALYSIS. The procedures used in data analysis are described. The particularly important questions of NC and CC identification and the elimination of backgrounds are discussed. 14

V. COMPARISON OF NC AND CC. Results for NC are given but always in the context of comparison with the much better known CC. 36

I. INTRODUCTION

Inelastic neutrino interactions can be divided into two processes, the charged current reaction (CC):

$$\nu_\mu \begin{pmatrix} p \\ n \end{pmatrix} \rightarrow \mu^- \begin{pmatrix} x^{++} \\ x^+ \end{pmatrix} \qquad (1)$$

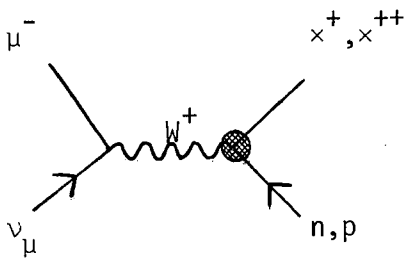

and the neutral current reaction (NC):

$$\nu_\mu \begin{pmatrix} p \\ n \end{pmatrix} \rightarrow \nu_\mu \begin{pmatrix} x^+ \\ x^o \end{pmatrix} \qquad (2)$$

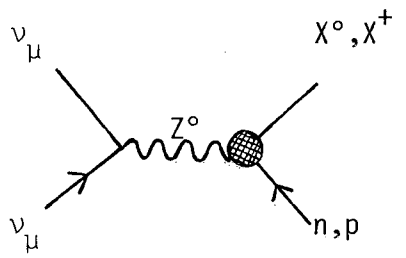

The target is either a proton (p) or a neutron (n) and the final state is a system of particles x with the charge indicated. The Feynman graphs to the right of each reaction represent the process pictorially. On the left hand side the leptons (particles without strong interactions) form a current $\nu_\mu \rightarrow \mu^-$ (CC) or $\nu_\mu \rightarrow \nu_\mu$ (NC). The hadrons (particles with strong interactions) similarly form a current that is either charged $\begin{pmatrix} p \\ n \end{pmatrix} \rightarrow \begin{pmatrix} x^{++} \\ x^+ \end{pmatrix}$ or neutral $\begin{pmatrix} p \\ n \end{pmatrix} \rightarrow \begin{pmatrix} x^+ \\ x^o \end{pmatrix}$. The two currents interact with the exchange of a weak vector boson W^+ for CC and Z^o for NC. The vertex where the weak vector boson joins the hadronic current is shaded to indicate the incomplete knowledge of the interaction. In contrast,

the lepton vertex is well understood and therefore not shaded. The process of lepton-nucleon scattering is often thought of as probing the unknown hadronic current with a known leptonic current.

The understanding of the NC has proceeded in two steps. The first step was to establish the existence of the NC. Until the early 1970's the weak force was studied by observing the decays of otherwise stable particles. Neutral current effects that could be investigated were possible strangeness changing neutral current decays of some strange particles. In particular, an extensive study was made of

$$K_L^0 \rightarrow \mu^+\mu^-$$

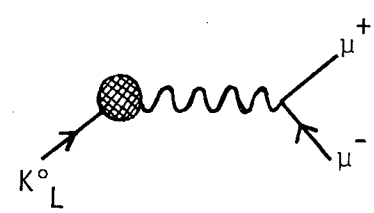

This strangeness changing neutral current process was found to be considerably less probable than the usual strangeness changing charged current.[1] With the availability of accelerator produced neutrino beams the neutral current process (2), which does not change strangeness, was first observed, and the rate was found to be comparable to CC.[2] The mere existence of the neutral current was a fundamental step in understanding the weak force.

The study of the neutral current has proceeded now to the second step: understanding how the neutral current couples to known particles. In the reaction (2) understanding the neutral current coupling amounts to understanding the shaded region where the Z^0 couples to the hadronic current. The generally complicated behavior of the coupling is greatly

simplified by the quark parton model, which is applicable at the high neutrino energies available at Fermilab. According to the model, hadrons consist of parts (partons), which are identified as the usual quarks. For example, the proton consists of two u(up) quarks and one d(down) quark and a sea of quark-anti-quark pairs. In the quark parton model lepton-nucleon scattering is described as simple lepton-quark elastic scattering. The complicated hadronic structure of the nucleon can be expressed in terms of momentum distributions of the quarks within the nucleus. Within the quark parton model, the goal of the study of NC is to determine how neutrinos scatter elastically from quarks. For each type (or flavor) of quark two constants are required to describe the elastic scattering.

This thesis will place some restrictions on possible values of the constants for the u and d quarks. The results will not be sensitive to the neutral current couplings of the s (strange) and c (charm) quarks since these quarks do not exist in the proton or neutron except in the quark-anti-quark sea.

Previous experiments[3] have studied the neutral current most successfully by measuring its rate compared to CC in both neutrino and anti-neutrino reactions. This experiment examines the nature of the final hadronic state with the detailed information available from the Fermilab fifteen foot bubble chamber and is the first experiment to study the individual hadronic particles in the final state at Fermilab energies.

II. THEORETICAL DESCRIPTION - QUARK PARTON MODEL

Neutrino nucleon inelastic scattering can be described with a simple quark parton model.[4] The main results of the model are summarized below. Consider the CC process of scattering a neutrino from an unpolarized spin 1/2 lepton (ℓ)

$$\nu_\mu \ell \rightarrow \mu^- \ell' \tag{3}$$

The matrix element may be written as

$$T = \frac{G_F}{\sqrt{2}} \; \overline{\psi}_{\mu^-} \; \gamma^\alpha (1-\gamma_5) \; \psi_{\nu_\mu} \overline{\psi}_{\ell'} \; \gamma_\alpha \; (1-\gamma_5) \; \psi_\ell \tag{4}$$

where the usual V-A coupling has been assumed for the particle fields ψ_{μ^-}, ψ_{ν_μ}, $\psi_{\ell'}$ and ψ_ℓ and G_F is the Fermi coupling constant. Conventional techniques may be used to derive the cross-section

$$\frac{d\sigma_{\nu\mu^-}}{d(\cos\theta)} = \frac{G_F^2 s}{2\pi} \tag{5}$$

where θ is the center of mass scattering angle and s is the center of mass energy squared. Similarly for the anti-neutrino process

$$\bar{\nu}_\mu \ell' \rightarrow \mu^+ \ell \tag{6}$$

The cross-section is given by

$$\frac{d\sigma_{\bar{\nu}\mu+}}{d(\cos\theta)} = \frac{G_F^2 s}{2\pi} \left(\frac{1+\cos\theta}{2}\right)^2 \tag{7}$$

In the parton model the scattering angle θ is conventionally replaced by the variable

$$y = \frac{2q\cdot p}{s} = \frac{1-\cos\theta}{2} \tag{8}$$

where $q = (k-k')$ is the momentum transfer and k, k', and p are the 4-momenta of the incoming neutrino, outgoing muon, and target lepton respectively. Thus (7) becomes

$$\frac{d\sigma_{\bar{\nu}\mu+}}{dy} = \frac{G_F^2 s}{\pi} (1-y)^2 \tag{9}$$

Similarly it can be shown that the scattering of $\bar{\ell}$, the anti-particle of ℓ, is described by (9) for neutrino scattering and (5) for anti-neutrino scattering.

The NC cross-section

$$\nu\ell \rightarrow \nu\ell \tag{10}$$

is not as well known because of the uncertainties in the form of the neutral current. The current is usually taken to be of the form:

$$J_\alpha = \frac{G_F}{\sqrt{2}} (C_V - C_A)\ \bar{\psi}_\ell\ \gamma_\alpha (1-\gamma_5)\ \psi_\ell + (C_V + C_A)\ \bar{\psi}_\ell\ \gamma_\alpha (1+\gamma_5)\ \psi_\ell \tag{11}$$

with $C_V - C_A$ and $C_V + C_A$ constants which describe the relative strengths of the two terms. The constants C_V and C_A will, in general, be different for different particles. For left-handed neutrinos the second term on the right vanishes because $(1+\gamma_5)$ is the projection operator for right-handed neutrinos. Right-handed neutrinos are not required by any experimental data and are therefore normally assumed not to be present. Thus, for neutrinos (11) reduces to the same V-A coupling found for CC, but for other particles $C_V + C_A$ may not be zero. The cross-section for the NC process is then:

$$\frac{d\sigma_{\nu\nu}}{dy} = \frac{G_F^2 s}{\pi}\left[(C_V-C_A)^2 + (C_V+C_A)^2(1-y)^2\right] . \qquad (12)$$

Similarly anti-neutrino scattering is given by:

$$\frac{d\sigma_{\bar{\nu}\bar{\nu}}}{dy} = \frac{G_F^2 s}{\pi}\left[(C_V-C_A)^2(1-y)^2 + (C_V+C_A)^2\right] \qquad (13)$$

The parton hypothesis models the proton as a collection of spin 1/2 particles. In the limit $s \to \infty$ the partons behave like free, structureless fermions and therefore scatter from neutrinos according to the cross-sections given above. The quark model identifies the partons as the usual four quarks: u,d, s and c. The proton consists of two u quarks, one d quark, and a sea of quark-anti-quark pairs. Because this experiment is not sensitive to the types of quarks in the sea, s and c quarks are neglected. The generalization to include them and other quark flavors, however, is straightforward. To compute the inelastic cross-section all that need be known is the momentum distribution of the quarks in the nucleus. In the ν-quark center of mass, where the proton has high momentum P, the probability of finding a u quark with momentum between xP and (x+dx)P is defined as u(x). The functions $\bar{u}(x)$, d(x) and $\bar{d}(x)$ are similarly defined but for u anti-quarks, d quarks and d anti-quarks respectively.

Neutrino charged currents raise the quark charge by one and therefore scatter from d quarks (charge -1/3) and produce u quarks (charge +2/3) or scatter from $\bar{u}$ quarks (charge -2/3) and produce $\bar{d}$ quarks (charge +1/3). The cross section for inelastic neutrino proton scattering may then be written as

$$\frac{d\sigma_{\nu\mu^-}}{dxdy} = \frac{xsG_F^2}{\pi} [d(x) + \bar{u}(x)\ (1-y)^2] \tag{14}$$

where s in (5) has been replaced by xs, the center of mass energy squared of the colliding parton and neutrino. The normalization of the functions is:

$$\begin{aligned} &\int [u(x) - \bar{u}(x)]\ dx = 2 \\ &\int [d(x) - \bar{d}(x)]\ dx = 1 \end{aligned} \tag{15}$$

In neutral current processes neutrinos can scatter from either u or d quarks. The cross-section for NC on a proton target is:

$$\frac{d\sigma_{\nu\nu}}{dxdy} = \frac{xsG_F^2}{\pi} [d(x)\ f(y) + u(x)\ f'(y) + \bar{d}(x)\ \bar{f}(y) + \bar{u}\ (x)\ \bar{f}'(y)] \tag{16}$$

where

$$\begin{aligned} f(y) &= (C_V-C_A)^2 + (C_V+C_A)^2\ (1-y)^2 \\ \bar{f}(y) &= (C_V+C_A)^2 + (C_V-C_A)^2\ (1-y)^2 \\ f'(y) &= (C_V'-C_A')^2 + (C_V'+C_A')^2 (1-y)^2 \\ \bar{f}'(y) &= (C_V'+C_A')^2 + (C_V'-C_A')^2 (1-y)^2 \end{aligned} \tag{17}$$

The neutron is related to the proton by an I-spin rotation. This rotation transforms u quarks into d quarks and vice versa. Thus, the function u(x) describes d quarks in the neutron and d(x) describes u quarks in the neutron. It then follows that the cross-sections for scattering from neutrons are just (14) and (16) with u and d interchanged. The scattering of neutrinos from targets with equal numbers of neutrons and protons is the average of the two: for CC

$$\frac{d\sigma_{\nu\mu^-}}{dxdy} = \frac{xsG_F^2}{2\pi} \left[\left(u(x) + d(x)\right) + \left(\bar{u}(x) + \bar{d}(x)\right) (1-y)^2\right] \tag{18}$$

and for NC

$$\frac{d\sigma_{\nu\nu}}{dxdy} = \frac{xsG_F^2}{2\pi} \left[\left(u(x) + d(x)\right) \left(f(y) + f'(y)\right) + \left(\bar{u}(x) + \bar{d}(x)\right) \left(\bar{f}(y) + \bar{f}'(y)\right)\right] \tag{19}$$

The quark model may also be used to describe the fragmentation of the quarks into the hadrons which are experimentally observed. The function $D_q^h(z)$ is the probability that an energetic quark q of momentum P will fragment into a hadron, h, of momentum between zP and (z + dz) P. The normalization of $D_q^h(z)$ is

$$\int_{z_{min}}^{1} D_q^h(z)\, dz = N_h \tag{20}$$

where N_h is the average number of hadrons of type h and $z_{min} \sim M_N/W$ where W is the mass of the hadrons produced and M_N is the nucleon mass. The behavior $D_q^h(z) \sim 1/z$ as $z \to 0$ will thus provide a hadronic multiplicity which rises logarithmically with W. The inclusive cross-section for production of a hadron h from protons via CC, for example, is

$$\frac{d\sigma^h_{\nu\mu^-}}{dxdydz} = \frac{xsG_F^2}{\pi}\left[d(x)\, D_u^h(z) + \bar{u}(x)\, D_{\bar{d}}^h(z)\, (1-y)^2\right] \tag{21}$$

Relations between the D functions follow from I-spin and charge conjugation symmetry. For example:

$$D_u^{\pi^+}(z) = D_d^{\pi^-}(z) = D_{\bar{u}}^{\pi^-}(z) = D_{\bar{d}}^{\pi^+}(z) \tag{22}$$

and

$$D_d^{\pi^+}(z) = D_u^{\pi^-}(z) = D_{\bar{d}}^{\pi^-}(z) = D_{\bar{u}}^{\pi^+} . \tag{23}$$

Using these relations the inclusive pion production CC cross-sections from targets containing equal numbers of neutrons and protons may be written as:

$$\frac{d\sigma_{\nu\mu^-}^{\pi^+}}{dxdydz} = \frac{xsG_F^2}{2\pi}\left[\left(u(x) + d(x)\right) + \left(\bar{u}(x) + d(x)\right)(1-y)^2\right] D_u^{\pi^+}(z). \tag{24}$$

For NC

$$\frac{d\sigma_{\nu\nu}^{\pi^+}}{dxdydz} = \frac{xsG_F^2}{2\pi}\Big[\left(u(x) + d(x)\right)\left(f(y)D_d^{\pi^+}(z) + f'(y)\ D_u^{\pi^+}(z)\right) + \left(\bar{u}(x) + \bar{d}(x)\right)\left(\bar{f}(y)D_{\bar{d}}^{\pi^+}(z) + \bar{f}'(y)D_{\bar{u}}^{\pi^+}(z)\right)\Big] \tag{25}$$

or, equivalently,

$$\frac{d\sigma_{\nu\nu}^{\pi^+}}{dxdydz} = \frac{xsG_F^2}{2\pi}\Big[\left(\left(u(x) + d(x)\right) f(y) + \left(\bar{u}(x) + \bar{d}(x)\right)\bar{f}'(y)\right)D_d^{\pi^+}(z) + \left(\left(u(x) + d(x)\right) f'(y) + \left(\bar{u}(x) + \bar{d}(x)\right)\bar{f}(y)\right)D_u^{\pi^+}(z)\Big] . \tag{26}$$

The parton model does not describe the distribution of hadron momenta perpendicular to the direction of motion of the fragmenting quark. However, the transverse momentum is limited: average transverse momenta are approximately 300 MeV/c for π's and 400 MeV/c for k's and p's.

III. EXPERIMENTAL ARRANGEMENT

The experiment described in this work is Fermilab Experiment 28. Other results from this experiment have been reported previously.[5] The 300 GeV/c proton beam was extracted from the accelerator and impinged on an aluminum target 1 mean free path in length. The positive secondaries were focused (negatives were defocused) by the horn.[6] The horn is a pulsed magnet which produces a toroidal magnetic field about the axis defined by the incoming proton beam. The horn design provides a large aperature (30 cm) and focuses in both the horizontal and vertical planes in a single element. After being focused by the horn the mesons produce neutrinos in a 400 meter long decay tunnel predominantly through the decay modes $\pi^+ \rightarrow \mu^+ \nu_\mu$ and $K^+ \rightarrow \mu^+ \nu_\mu$, the K^+ decays producing the higher energy neutrinos. At the end of the decay tunnel the decay muons are completely absorbed by 1 Km of earth shielding while the neutrinos pass through the shielding with no appreciable attenuation. The neutrino beam produced is a wide band beam--the observed energy spectrum is shown in figure 1. The method used to obtain figure 1 will be described later.

The detector for this experiment was the Fermilab fifteen foot bubble chamber[7] and the External Muon Identifier (EMI). The bubble chamber was filled with a 21% atomic mixture of neon in hydrogen. This mixture, a so-called light mixture, had a density of 0.28 g/cm^3 and a collision length of 210 cm. This relatively short collision length, comparable to the bubble chamber radius of 1.9 meters,[8] allowed some of the hadrons to be identified by their interactions in the bubble chamber. The

magnetic field at the center of the bubble chamber was 30 Kg. The radiation length in this mix was 110 cm. This radiation length provides modest π° identification -- both γ's from the decay $\pi^\circ \rightarrow \gamma\gamma$ are converted about 1/3 of the time. The energy loss for a minimum ionizing particle was 2/3 MeV/cm.

Figure 2 is a schematic of the 15' bubble chamber and EMI. Details of the operation and calibration of the EMI have been published previously.[9] The EMI consists of a thin 3-5 absorption length hadron absorber downstream of the bubble chamber followed by a single plane of multiwire proportional chambers. To use the EMI, the trajectory of a muon candidate which has been measured in the bubble chamber is extrapolated through the magnetic field to the proportional chambers. If the track is a muon, the extrapolated position will usually match closely with the position reconstructed from the proportional chamber data. Hadrons, however, will usually scatter in the absorber and the positions extrapolated from the bubble chamber measurements and the positions observed in the proportional chambers will not generally agree. These expectations can be made quantitative by defining C_μ, the probability that a muon would have a worse match between the extrapolated position and the position determined from the proportional chamber data. Explicit formulas for the calculation of C_μ and distributions in C_μ for hadrons and muons are given in reference 9.

IV. ANALYSIS

1. Scanning

The bubble chamber film was scanned for all interactions with two or more outgoing tracks produced by an incident neutral particle. The major problem in scanning for these events is that any given event topology can be considered as an event with an incident neutral particle or an event with an incident charged particle and one fewer outgoing charged particles. Events were classified as having an incident charged particle and were rejected if any one of the following criteria was met:

1. One of the tracks was shown to be incident by one or more energetic recoil electrons (δ-rays). The direction of the δ-ray is required by kinematics to be in the direction of motion of the track and thus unambiguously defines the track direction. The projected radius of curvature of the δ-ray was required to be greater than 3 mm which corresponds to a momentum of about 3 MeV.

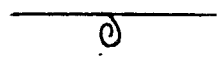

δ-ray direction

2. One of the tracks was headed upstream (if interpreted as coming from the interaction vertex) and had a radius of curvature on the scanning table greater than 90 cm. Since the demagnification of the 15' bubble chamber optical system is not constant but varies with depth, distances on the scanning table

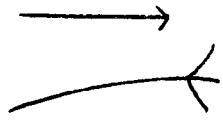

radius > 90 cm

vary between 1/2 and 1/8 of the corresponding distance in space. The radius of curvature of 90 cm therefore corresponds to a projected momentum of 1.6 - 7.2 GeV/c depending on the depth in the chamber.

3. The event had 2 prongs and the opening angle was greater than 90°. This criterion eliminated many charged particle scatterings from neutrons.

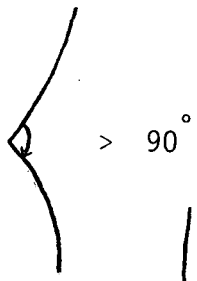

4. The event had 3 prongs, including two tracks of opposite charge which were longer than 5 cm on the scanning table and had an opening angle of 175° or more. This criterion eliminated many charged particle elastic scatterings from protons.

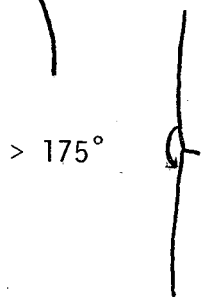

All events which met the scan criteria were recorded for measurement. The scan rules required the inclusion of many events which did not have an incident neutral track. The rules, however, were not expected to reject a significant number of neutrino events. Criteria 1) and 2) cause no loss of neutrino events. Criteria 3) and 4) are unlikely to be satisfied by neutrino events because the hadrons generally emerge from the reaction in the forward direction in a narrow cone due to the limited transverse momentum distribution. The loss due to rules 3) and 4) is estimated by Monte Carlo to be less than 1%.

A second scan on a portion of the film estimated that the efficiency of the first scan was 91%. The scan inefficiency may

have been partly due to the fact that portions of the chamber wall were coated with ice or other solids. The ice coating had the effect of decreasing the contrast between tracks and the background and therefore reducing event visibility.

2. Measuring

Recorded events were measured on a film plane digitizing device called a Franckenstein. All charged tracks at the primary vertex were measured. Downstream vees (including γ's converted into e^+e^- pairs) were measured if they could have come from the primary vertex, i.e., if they "pointed" to the primary vertex. The pointing test consisted of a judgement made during the scanning as to whether the hypothesized line of flight of the neutral track passed between the two charged tracks forming the vee. Downstream neutron or K_L° interactions were measured as separate events if they satisfied the scanning criteria. Other interactions were not measured.

An important feature of the measurement process was that every track was given a label describing its fate. A track was called "interacting" if it had visible interaction in the bubble chamber with one or more outgoing prongs. A track was called "ending" if the track did not leave the bubble chamber and if no other label was applicable. A track was called "electron" if it spiralled to a point (implying minimum energy loss at low momentum -- say below 30 MeV/c-- hence identifying the particle as an electron). A track was also called "electron" if it showed signs of energy loss due to bremsstrahlung: a sudden change in track curvature or a γ converted

into an e^+e^- pair with the line of flight of the γ tangent to the track in question. Decays of π mesons from rest were labeled if the track had a kink followed by a short track (a μ with a range of about 0.4 cm in space) and electron which spiralled to a point. Possible muon decays were also labeled, but the category "μ decay" included both μ decays and π decays where the $\pi \rightarrow \mu$ decay was not seen. Tracks which did not satisfy any of the above criteria were called "leaving." No track was given more than one label. The labeling is summarized in Table I.

Seven percent of the events were judged unmeasurable. Some of them were unmeasurable because the vertex was obscured, out of the field of view in some view, or badly focused. Other events were unmeasurable because of a secondary interaction or a converted γ close to the primary vertex. Often a combination of factors was responsible for events not being measured.

3. General Analysis Procedures

The measured events were processed through the geometry computer program TVGP.[10] The data from the EMI proportional chambers was processed through the program SID.[11] A modification to TVGP allowed the EMI information to be integrated with the bubble chamber information. The measured vees were fitted with the program SQUAW.[12]

Events were required to pass successfully through the geometry program TVGP. This requirements produced a 14% event loss. Those events whose total visible momentum in the direction of the neutrino beam (ΣP_x) was less than 1 GeV/c were eliminated. The events with $\Sigma P_x < 1$ GeV/c are expected to comprise 4% of all neutrino events.

However, no events were lost by this cut which would not have been lost by the cut in visible energy of 5 GeV which was made later. The purpose of this cut was to eliminate most of the events which had an incoming charged particle but had not been rejected by the scanning criteria. Events in a fiducial volume of 21 m^3 were selected for further analysis. This fiducial volume required that the primary vertex of the event be further than 5 cm from the nearest portion of the wall and further than 35 cm from the downstream portion of the wall. Events where EMI information was not available were also eliminated, causing a 3.5% loss of events. A summary of the preliminary event selection criteria is given in Table II.

4. Charged Current Selection

The EMI was used to identify CC reactions (1) by the presence of a muon in the final state. Some confusion between CC and NC reactions may arise if the hadronic state X contains one or more muons. Such muons are expected from the production of charmed particles, but the expected rate ($\sim$1% of total neutral current cross-section)[13] is sufficiently small as to have no influence on the conclusions drawn in this work.

The decays of π or K mesons is not a problem either because of their long decay lengths. On the average there is one leaving negative hadron per neutrino event. At 3 GeV/c the π has a decay length of 170 meters. The probability of a decay in the space of 2 meters between the bubble chamber and the EMI is 1%. Below 3 GeV/c a much larger fraction of the π's decay but they do not create a problem because no

attempt is made to identify muons below 3 GeV/c. In fact, the 1% contamination is an upper limit because: 1) 3 GeV/c is the lower limit on the tracks considered for identification, and 2) the π decay will cause a momentum change in the track so the trajectory will, in general, not correspond closely to the trajectory expected from the extrapolation of the bubble chamber track.

The most serious problem in the identification of charged currents is the proper interpretation of the EMI data. The separation of hadrons and muons by the EMI is far from complete due to several inadequacies in the EMI. First, the absorber is thin: 5% of the hadrons pass through the absorber without scattering. Second, the proportional chambers are only 95% efficient. The inefficiency is due largely to cases where many tracks -- about 5 or more -- cross the proportional chamber in a single pulse. The third problem is that tracks unrelated to the neutrino event may traverse the proportional chambers and match the extrapolated positions of some track in the neutrino event. Reference 9 describes how these effects are incorporated into the definition of C_μ. By definition the distribution of muons in C_μ will be flat. Hadrons will be concentrated at small values of C_μ. However, for a sample of tracks considered in reference 9 the fraction of hadrons with $C_\mu > 0.1$ was 16%. Thus the separation of hadrons and muons is reliable on a track by track basis only to 80-90%.

It is, however, possible to use the statistical description of the EMI to make an accurate count of the number of muons in any given sample. A method has been developed that defines an estimator ϕ_i for the ith track. The ϕ_i average to 1 for muons and to 0 for hadrons. Thus $\sum_i \phi i$ is a measure of the muon content of the sample. The details of the method are given in the Appendix.

The geometric acceptance of the EMI is 86% for the neutrino spectrum observed. Half of the loss occurs at low muon energies where the muons are swept out of the EMI acceptance by the bubble chamber field (30 Kg) while the other half is due to muons passing above or below the array of proportional chambers. The geometric acceptance has been calculated by Monte Carlo. The results of the Monte Carlo may be parameterized by:

$$A = \begin{cases} (0.95 - 1.78 \sin^2\theta) \quad \exp\left(\frac{-1.6}{p}\right)^{3.5} & \sin\theta < 1/2 \\ (1.13 - 1.25 \sin\theta) \quad \exp\left(\frac{-1.6}{p}\right)^{3.5} & \sin\theta > 1/2 \end{cases} \tag{27}$$

where A is the acceptance averaged over position within the bubble chamber, and p and θ are the track momentum in GeV/c and angle with respect to the neutrino beam. Each track was weighted by ϕ_i times the reciprocal of the acceptance. As is apparent from (27) A decreases rapidly below a momentum of 3 GeV/c. Because of the large corrections that would have been required, no attempt was made to identify muons below 3 GeV/c. To correct the distributions for undetected muons below 3 GeV/c a Monte Carlo program was employed.

5. Monte Carlo

The Monte Carlo[14] generates events in neutrino energy E_ν according to the observed neutrino beam spectrum (figure 1). Then the muon (or outgoing neutrino in NC) energy and angles are generated according to

to the x and y distributions for neutrino events (equations 15 and 16) with:

$$x\left(u(x) + d(x)\right) = 2.61\ \sqrt{x}(1-x)^3 - 2.51\ \sqrt{x}\ (1-x)^5 + 15.60\ x^{\ 0.85}\ (1-x)^9 \tag{28}$$

and

$$x\left(\bar{u}(x) + \bar{d}(x)\right) = 0 \tag{29}$$

where the x distribution is a fit by Barger[15] to high energy neutrino data. For NC the possibilities $f(y) + f'(y) = 1$ and $f(y) + f'(y) = (1-y)^2$ are considered separately, the more general case being a linear combination of the two (compare with eqn. 19). The events are generated uniformly throughout the fiducial volume. From Monte Carlo calculations of the beam spectrum the neutrino flux is expected to be very nearly uniform throughout the fiducial volume, and the observed distribution is consistent with this expectation. The target nucleon is chosen to be a neutron 1.6 times more often than a proton for charged currents and 1.1 times more often for neutral currents. These numbers are consistent with the total cross-section ratios for neutrons and protons quoted in this work.

The variables E_ν, x, and y determine the momentum and mass of the hadron system. However, the number, type, and momenta of the hadrons must be specified. The Monte Carlo generates the number of particles n according to a probability distribution P(n) proposed by Czyzewski and Rybicki.[16]

$$P(n) = \frac{.141\ (1.8)^{3.6d + 6.48}}{.8\bar{n}\ \Gamma\ (1.8d + 4.24)} \quad \text{for } 1 \leqslant n \leqslant 15 \tag{30}$$

where

$$d = 2.5\ \frac{n-\bar{n}}{\bar{n}}$$

$$\bar{n} = 3/2\ (1.09 + 1.09\ \ln W^2) \tag{31}$$

and Γ is the standard gamma function. The mean multiplicity, $\bar{n}$, is 3/2 times the charged multiplicity observed by Chapman, et. al.,[17] in a high energy neutrino scattering experiment with a hydrogen target. The factor 3/2 is intended to account for neutral particles.

Each final hadronic state contains either a neutron or a proton and pions. Since the major use of the Monte Carlo is to model the

fraction of energy that appears in the charged particles, it is not important to generate the relatively small number of K_S° and Λ that are observed. The baryon is chosen to be a neutron or proton with equal probability except for the reactions of the type:

$$\nu p \rightarrow \nu B \tag{32}$$

and

$$\nu p \rightarrow B \pi \mu^- \tag{33}$$

where the baryon, B, must be a proton to satisfy charge conservation. After the baryon charge is selected, the π's are initially assigned the sign of charge required to conserve the total charge. If, after balancing the charge, an odd number of π's remain, one π is assigned charge zero. The even number of π's that then remain are divided between $\pi^+\pi^-$ and $\pi^\circ\pi^\circ$ pairs in the ratio 2:1.

The momentum of the individual hadrons is given by phase space times a distribution which limits transverse momentum. Specifically

$$\frac{dN}{dp_t^2} \alpha\ e^{-bp_t^2} \text{ x phase space} \tag{34}$$

with $b = 6.25 \frac{n-1}{n} (\mathrm{GeV/c})^{-2}$ where n is the number of particles in the hadronic final state, and p_t is the transverse momentum relative to the total hadron direction. A method for the Monte Carlo generation of this distribution has been given by Van Hove.[18]

6. E_ν, E_{vis}, v and y_{vis} Distributions for CC Data

To produce a distribution of CC events the following steps are followed:

1. Interpret each non-interacting negative track with momentum greater than 3 GeV/c as a muon and find the weight ϕ_i as described in the Appendix.
2. Calculate the variable of interest interpreting that track as the muon. Make a histogram of the variable with weight ϕ_i for each possible muon. Calculate the errors as described in the Appendix.
3. Correct each bin of the histogram for $p_\mu < 3$ GeV/c, where the corrections are determined by the Monte Carlo.

The distribution in neutrino energy (Figure 1) was obtained using the above and the Myatt method[19] to determine the neutrino energy. The Myatt method estimates the energy of the missing neutrals using the assumption that the momentum vector of the neutral particles is in the same direction as the charged hadronic particles. The hadron momentum vector is projected into the plane defined by the incoming neutrino and outgoing muon. The projected hadron momentum is then scaled so that it balances the muon momentum perpendicular to the neutrino beam direction. If the scale factor is negative it is a

"failure" and is not considered further. For neutrino events which are not failures the neutrino momentum is given by the vector sum of the muon momentum and the scaled, projected hadron momentum vector. The observed beam spectrum served as input to the Monte Carlo. The process was an iterative one because figure 1 itself requires Monte Carlo corrections for $p_\mu < 3$ GeV/c.

It would be ideal if this experiment could measure E_ν, x and y directly. However, because some neutral particles are not detected the total energy is not observed. For CC events several methods, such as the Myatt method, have been devised to estimate the missing energy. However, no reliable method of estimating the missing energy in neutral currents is known. For this reason, this work will from now on use variables which may be calculated from observed quantities without assumptions.

The distribution in E_{vis} depends on the neutrino energy, the charges of the hadrons and, to some extent, their masses. Since the masses of the particles are not normally known, E_{vis} is defined simply as

$$E_{vis} = \sum_i p_i + \sum_k \left(\sqrt{p_k^2 + M_p^2} - M_p \right) \tag{35}$$

where p_i and p_k are the lab momenta of the ith and kth particles respectively. The second sum extends over all protons which stop in the bubble chamber while the first extends over all other particles.

The use of the form in the second sum of (35) avoids an over-estimate of the neutrino energy E_ν in some events having a large number of low momentum protons due to the breakup of a neon nucleus. The distribution in visible energy is given in figure 3. The agreement with the Monte Carlo (solid line on figure 3) is satisfactory. The χ^2 is 13.6 for 8 degrees of freedom.

The variable y_{vis} is defined in a way analogous to y:

$$y_{vis} = \frac{E_{vis} - p_\mu}{E_{vis}} \tag{36}$$

where p_μ is the laboratory muon momentum. Its distribution is given in figure 4. It is possible to determine the y distribution f(y) for charged currents from the y_{vis} distribution. To do so, however, requires heavy reliance on the Monte Carlo. The Monte Carlo has been used to generate distributions for both f(y) = 1 (appropriate for quarks) and $f(y) = (1-y)^2$ (appropriate for anti-quarks) and these distributions are the solid curves on figure 4. The best fit to the data with the form $1 - \varepsilon + 3\varepsilon\,(1 - y)^2$ is given by $\varepsilon = .16 \pm .04$ with a χ^2 of 25 for 8 degrees of freedom. The dashed curve is the best fit to the data.

The confidence level of the fit is 0.1%, a value which suggests that systematic errors are important. One possible interpretation is that the data are systematically low at large y_{vis}. This could be because: 1) muon identification is biased at low muon momentum

(which corresponds to large y_{vis}) or 2) the Monte Carlo overestimates the amount of hadronic energy that is visible. The method of muon identification is known to be accurate to 1 ± 2% for muon momenta above 10 GeV/c. It has not been possible to test the method directly below momenta of 10 GeV/c, but the number of muons counted is not sensitive to a variation of the parameters in the expression for C_μ (see Appendix and reference 9). The Monte Carlo is much more suspect. Possible problems with the Monte Carlo are that: 1) the ratio of charged to neutral particles and hence the visible energy may be overestimated 2) the γ detection efficiency may be overestimated (largely because of scanning inefficiency), or 3) nuclear effects, which have been neglected, may affect the fraction of energy that is visible. To avoid dependence on the details of the Monte Carlo, the neutral current events are compared directly with the charged current events. The Monte Carlo is used to make modest (25%) corrections to the CC data for low energy muons (P_μ < 3 GeV/c), which are not detected.

While both x and y depend on the neutrino energy, the variable $v = xy$ does not. The variable v depends only on the muon momentum and angle. The v distribution is shown in Figure 5 and should be compared with the Monte Carlo curve. The agreement between Monte Carlo and data is good (χ^2 = 13.7 for 11 degrees of freedom).

It can thus be concluded that the Monte Carlo provides a satisfactory description of the data and that it is reasonable to use the Monte Carlo to correct for the loss of low energy muons (p_μ < 3 GeV/c). Equivalently, the CC distributions agree with the known properties of neutrino interactions since these properties were the input to the Monte Carlo.

7. Selection of Neutral Current Events

The selection of NC is very different from the selection of CC. For NC the approach is to eliminate the known sources of backgrounds and to attribute the residual events to NC. In addition to several minor backgrounds, there are two potentially very serious backgrounds in the sample of NC: CC and events due to the interaction of neutral hadrons.

a. CC background

The CC are a serious background not only because they are more numerous (by a factor of 3), but also because of their distribution in visible energy. From present data the ratio of NC to CC appears to be independent of neutrino energy but does depend strongly on visible energy for the following reason. Typically, most of the neutrino energy will be visible in the final state of a CC, but somewhat less than half the energy will be visible in a NC. The difference, of course, is that in NC the outgoing neutrino carries away a large fraction of the energy. The fact that NC have a considerably smaller fraction of energy that is visible means that the ratio of CC to NC will be considerably larger than 3 at the higher visible energies and considerably smaller at the lower visible energies. As will be discussed later, the neutral hadron background is very large at the lower energies, so it is necessary to study neutral currents at the higher visible energies, where the CC background is potentially large.

The selection used to reject CC is that the negative track with the highest transverse momentum with respect to the neutrino beam

must interact or decay[20] in the bubble chamber. This criterion is effective because the muon in CC events is nearly always the negative particle with the highest transverse momentum. To clarify this point the following argument is made. As can be seen from figure 6, the muon typically has 1-2 GeV/c momentum transverse to the neutrino beam direction. The hadron system must have an equal but opposite transverse momentum, but it is spread over several (typically 5) hadrons. Since each of these particles will have small (~300 Mev) transverse momentum relative to the average hadron direction, the transverse momentum of a typical hadron is substantially less than that of the muon. Even with this selection the CC contamination remains substantial (25% of NC for E_{vis} > 10 GeV).

The residual CC contamination is difficult to eliminate. When the muon is not the highest in transverse momentum, it is generally also very low in momentum (below 3 GeV/c where the EMI is not effective). The procedure employed was to use the EMI to subtract events with muon momenta above 3 GeV/c and use the Monte Carlo program for events with lower muon momentum. Of course, the Monte Carlo program should agree with the data when the muon momentum exceeds 3 GeV/c. For the charged current sample of 1580 events, the Monte Carlo predicts 72 events in which the negative track with the highest transverse momentum is not the muon. Of these 72 events, 30 are expected to have a muon greater than 3 GeV/c and 25.1 ± 9.7 are observed with the EMI.

In NC the negative with the highest transverse momentum will always be a hadron, but it may not interact. The NC events must be weighted by the reciprocal of the probability that that negative track would have interacted. This probability is shown as a function of momentum in

figure 7. This figure was obtained by taking negative hadrons from charged current interaction and counting the fraction that interacted. Note that this procedure automatically takes into account scanning efficiency if scanning for interactions has the same efficiency for CC and NC. The probability in figure 7 depends strongly on momentum, not so much because of the variation in cross-section as in potential path length. At the lower momenta the particles tend to be trapped in the magnetic field and therefore have very long path lengths.

b. Electron neutrino background

There are several miscellaneous sources of background for NC. Events induced by electron neutrinos ν_e or anti-neutrinos $\bar{\nu}_e$ are a negligible contaminant. Approximately 1% of the beam is ν_e and 0.1% is $\bar{\nu}_e$.[21] In the case of the ν_e events the electron will be identified by bremsstrahlung losses (about 40% of the time) or will leave without interacting. In either case ν_e's will not be selected as neutral currents (the highest transverse momentum negative track will nearly always be the e^- and the e^- will not interact). The $\bar{\nu}_e$'s are too small a component of the beam to constitute an important background.

c. Charged hadron background

There is a small background due to interactions with incoming charged hadrons, even after the requirement $\Sigma P_x > 1$ GeV/c is imposed. These events are due either to: 1) badly measured tracks or 2) hadrons travelling upstream when they interacted. For this reason, events are eliminated if the sum of the momentum of all but one of the tracks in the event is between

20 and 100% (allowing for errors) of the momentum of the remaining track. More specifically events were eliminated if

$$|\vec{P}_+^j| > -\sum_{i\neq j} \vec{P}_-^i \cdot \frac{\vec{P}_+^j}{|\vec{P}_+^j|} > .2|\vec{P}_-^j| \quad \text{incoming hadron} \quad (37)$$

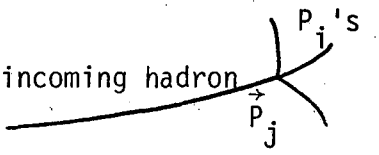

for any j. The momentum $\vec{P}_+^j$ ($\vec{P}_-^j$) is the momentum of the jth particle raised (lowered) by one standard deviation. The direction of all particles is taken to be away from the primary vertex. By performing the same test on hadrons in CC, it is estimated that this criterion loses less than 1% of the NC.

d. Antineutrino background

Another background of some importance is events due to $\bar{\nu}_\mu$ interactions. For these events the highest transverse momentum negative particle will frequently interact and these events would be in the NC sample unless eliminated by some other means. The charged current $\bar{\nu}_\mu$ background is eliminated by using the EMI to identify the outgoing μ^+. Specifically, an event was classified as an antineutrino if $y_{vis} < 0.5$ and $L > 3$ where L is the EMI likelihood ratio.[22] The likelihood ratio is the ratio of the probability that a muon would have a confidence level C_μ to the probability that a hadron would have a confidence level C_μ. The two criteria require some explanation. The choice $L > 3$ was made because it is less subject to negative fluctuations than the statistical estimator ϕ_i (ϕ_i is sometimes negative). The cut in y_{vis} was made to take advantage of the difference

between anti-neutrinos which occur mostly at small y_{vis} because of their $(1-y)^2$ distribution, and NC with a hadron with $L > 3$, which normally occur at large y_{vis} when the hadron is interpreted as a muon. Ten percent of the anti-neutrinos have $y_{vis} > 0.5$ and 5% of those with $y_{vis} < 0.5$ fail to be identified by the EMI. By performing the same test on hadrons in charged current events, it is estimated that 1% of the NC are lost by this criterion. The NC cuts discussed thus far are summarized in Table III. After these cuts 923 events remain, of which 280 are above 5 GeV/c in visible energy.

e. Neutral hadron background

The most severe background in this experiment is due to the interactions of neutral hadrons. The number of events with $\Sigma P_x > 1$ GeV/c which are not neutrino induced is comparable to the number of neutrino induced events. Fortunately, the background falls rapidly with increasing energy. The best measure of the hadron contamination comes from the events with evidence of upstream interactions. Hadronic particles must have been produced within the last few hadronic collision lengths of the material in front of the bubble chamber. Neutrinos, on the other hand, come from the π or K decay 1.0 - 1.4 Km away. In the case of the hadrons evidence of the upstream interaction which produced the hadron may be seen, but in the case of neutrino interactions all particles from the production process are absorbed by the muon absorber (except of course for the neutrinos themselves). The evidence of an upstream interaction may be direct: an interaction in the bubble chamber liquid of some other neutral or charged particle. But the evidence may very well be indirect: a concentration

of tracks emanating from a localized point on the wall, indicating an interaction in the wall, coils, support structure or elsewhere upstream. To take advantage of this difference a second scan was performed after the events had been measured. The scanner determined the direction of the momentum vector of the incoming neutral particle from the fastest tracks in the events. Using this direction the scanner looked for another event (including events in the wall) that could have produced the neutral. If a source for the neutral was found, it was called "associated". Otherwise, it was "not associated". The events were not usually ambiguous between "associated" and "not associated", but the distinction was a qualitative one.

In figure 8, the number of neutral current candidates as a function of energy are shown. Those events which were called associated have been shaded. The associated events fall more rapidly with increasing energy than do the unassociated events, implying that the importance of hadron background decreases with increasing energy.

With some simplifying assumptions the associated events may be used to evaluate the hadron background. The number of associated events, N_A, is given by

$$N_A = rN_H + fN_\nu \tag{38}$$

where r is the probability that a hadron will be associated, f is the probability that a neutrino will be accidentally associated, and N_H and N_ν are the number of hadron events and neutrino events respectively. The number of unassociated events is:

$$N_u = (1 - r)\, N_H + (1 - f) N_\nu \tag{39}$$

If r and f are known, (38) and (39) may be inverted to find N_H and N_ν.

The probability, r, that a hadron will be associated is found from the lowest energy bin in figure 8. In this bin there are expected to be only a few neutrino events. Assuming that the 431 events from 1-3 GeV in figure 8 are due to hadron background one obtains the average hadron association probability by dividing the number of associated events by the total: $r = 258/431 = .60 \pm .02$. Although this experiment does not observe the energy dependence of r, it is assumed that the energy dependence is small. The basis for this assumption is that hadronic cross-sections are quite constant above 1 GeV/c and that source of a 2 GeV/c hadron and the source of a 10 GeV/c hadron will be equally deep in the material in front of the chamber. The source of the 10 GeV/c hadron will then be equally likely to be visible as was the source of the 2 GeV/c hadron. However, it should probably be emphasized that the assumption that r does not depend on energy is not verified directly in this experiment.

The false association probability, f, is evaluated with CC and is assumed to be the same for NC. Figure 9 shows the fraction of charged current events which appear to be associated as a function of E_{vis}. Down to 5 GeV the fraction of events which appear to be associated is small. There is an apparent, but small, energy dependence to the charged current associations. To approximate the data, a false association probability of 0.1 below 20 GeV and 0.05 above 20 GeV was used for the NC rate as a function of energy. For samples in which all energies are used the average value of 0.067 ± .009 was used. Using (38) and (39) to solve for N_ν

$$N_\nu = \left(\frac{r}{r-f}\right) N_u + \frac{(r-1)}{(r-f)} N_A \qquad (40)$$

The procedure for using (40) is probably best explained by the example which follows.

V. COMPARISON OF CC AND NC

1. Neutral Current Rate

Table IV gives the details of the calculation of the number of NC as a function of energy. The first column (N) contains the 280 events above 5 GeV that remained after the cuts enumerated in Table III. Each event was weighted by the probability that the highest transverse momentum negative track would be identified as a hadron. The next two columns (N_u and N_A) contain the breakdown of events into unassociated (N_u) and associated (N_A). The next column (CC) is the number of charged currents detected by the EMI in the unassociated events. These CC events are subtracted from N_u to give N_u'. Using (40) with N_u' substituted for N_u, the number of neutrino events, N_ν, is evaluated using r = 0.6. Finally the charged current contamination with $p_\mu < 3$ GeV/c, as determined by the Monte Carlo, is subtracted. The last two columns give N_ν for other values of r (0.5 and 0.7) and show a lack of sensitivity (except for the lowest energy bin) to r.

The data are displayed in figure 10. The errors shown are statistical only, but the systematic errors are much smaller with the possible exception of the 5-10 GeV point. Below 5 GeV, the subtraction for hadron background is so large that the determination of the number of neutrino events, N_ν, is not reliable. For this reason, the visible hadronic energy, E_h, will be required to be greater than 5 GeV for all data presented below.

It is now possible to make a check on the corrections which have been made to the data. NC and purely hadronic events were identified because a nagative track interacted in the bubble chamber. CC were independently

identified using the EMI. Both the neutral and charged current data have been corrected for detection efficiency using Monte Carlo methods. An independent check on the procedures used is that the sum of CC, NC, and hadronic events should be equal to the number of events in the original sample. Above 5 GeV, the methods described above yield 1539 CC, 352 NC, and 143 hadronic events. Their sum is 2034±35 and is, within errors, equal to the 2016 events above 5 GeV which were in the original sample.

The ratio of NC to CC, R_ν (E_h), is obtained from figure 10, and is shown in figure 11. There are a number of small corrections and qualifications to the NC data which should be enumerated. First, the cuts listed in Table III lost some NC and did not eliminate all the background. It is estimated from the numbers in Table III that 2% of the NC are lost by cuts 2)-4) and that 3% of the NC sample is background from the sources 2)-4). A further background is neutral current events from anti-neutrinos. For a neutral current rate $R_{\bar{\nu}} = 0.4$,[23] the anti-neutrino neutral current events constitute a background of 6%. Most of these, however, are below 10 GeV; above 10 GeV the background is 2%. Also, this experiment does not observe the 0 and 1 prong reactions:

$$\nu n \rightarrow \nu n + \pi^0\text{'s}$$

$$\nu p \rightarrow \nu p + \pi^0\text{'s}$$

These two reactions are expected to contribute 5% of the NC cross-section for $E_h > 10$ GeV. To partially cancel the loss of 0 and 1 prong NC events 2 prong CC events are eliminated when comparing NC and CC. The 2 prong CC constitute 2.6% of all CC with $E_h < 10$ GeV..

The effects listed above amount to a net correction of less than 1%.

For $E_h > 10$ GeV on the hydrogen-neon target the ratio of NC to CC is found to be $R_\nu(E_h > 10) = .35 \pm .06$.

The ratio of NC to CC without the requirement $E_h > 10$ GeV depends on the y distribution of NC. The expected NC to CC ratio as a function of energy is indicated by the curves on figure 11 for flat and $(1-y)^2$ distributions. For a flat y distribution 40% of the NC have $E_h > 10$ GeV but for a $(1-y)^2$ distribution only 20% of NC have $E_h > 10$ GeV. For predominantly flat y distributions the correction to obtain R_ν without restriction on E_h is small. For example, for the y distribution $.9 \pm .3\ (1-y)^2$ (see discussion in section on u_{vis} below) the correction is only 5%.

The NC to CC ratio also depends on the relative numbers of neutrons and protons in the target because the ratio of cross-section on n and p targets is probably different for NC and CC. If it is assumed that the ratio of CC cross-sections on neutrons to CC cross-section on protons is 1.9, a number that follows from the x distributions of Field and Feynman[24], then the ratio of cross-sections for NC is $1.27 \pm .36$ as determined later in this work. The NC to CC ratio for a target with equal numbers of neutrons and protons is then 3% less than observed in this experiment.

The net effect of the corrections to the ratio of NC to CC is negligible so the ratio should be comparable to that observed in other experiments. The comparison is made in Table V, which shows that the ratio observed in this experiment is higher than, but compatible with, that observed by other experiments.

2. Momentum Imbalance

Thus far no evidence has been presented that there is a neutrino in the final state or even that the NC selected are different from CC. The momentum imbalance perpendicular to the neutrino beam provides a test, although a weak one, that there is a neutrino which carries a large transverse momentum. If there were no neutral particles at all in the final state the momentum imbalance would be zero (except for measurement errors). The outgoing neutrino (in analogy with the outgoing muon in CC) is expected to carry, on the average, larger transverse momentum than the hadrons (n, π°, K°), so NC are expected, on the average, to have greater momentum imbalance than CC. This expectation is borne out by the data shown in figure 12. The data in figure 12 rules out the possibility that a substantial portion of the neutral current sample above P_T = 1 GeV/c consists of misidentified CC.

3. u_{vis} Distribution

In NC the usual variables E_ν, x and y can be determined if the energy of the incoming neutrino and the masses and momenta of all the particles in the final hadronic state are known. However, in this experiment, the neutrino energy is not known and many of the neutral particles escape the bubble chamber. A useful variable, which depends only on the hadronic momentum and angle in the limit $E_\nu \to \infty$, is

$$u = x\,(1 - y) \tag{41}$$

and is analogous to $v = xy$, which depends only on the muon momentum and angle. The variable u can be expressed in terms of hadronic quantities with the help of

$$E_H = (ME_\nu y + M^2)/M \tag{42}$$

and

$$\sin^2\theta_H = \frac{2ME_\nu\ x(1-y) - M^2x^2y}{y\ E_\nu^2 + 2\ ME_\nu x}$$

where M is the nucleon mass, and E_H and θ_H are the energy and angle of the hadronic system in the laboratory frame.

In the limit $E_\nu \to \infty$

$$E_H \to y\ E_\nu \tag{44}$$

$$\sin^2\theta_H \to \frac{2Mx(1-y)}{y\ E_\nu} \tag{45}$$

and

$$u = \frac{E_H \sin^2\theta_H}{2M} \quad \text{as} \quad \frac{M}{E_\nu} \to 0 \tag{46}$$

This experiment does not observe the full hadronic system but only a portion of it. Therefore the variable u_{vis} is defined:

$$u_{vis} = \frac{E_h \sin^2\theta_h}{2M} \tag{47}$$

where the lower case h, which denotes visible quantities, distinguishes (46) from (47). In figure 13 the distribution in u_{vis} is shown for both NC and CC. The curve labeled "flat" was obtained by drawing a smooth curve through the CC data and normalizing it to the NC data. The curve labeled "$(1-y)^2$" is the "flat" curve divided by the ratio of the u_{vis} distribution expected for $f(y) + f'(y) = 1$ (c.f. eqn 19) to that expected for $f(y) + f'(y) = (1-y)^2$. This ratio was determined from the Monte Carlo using the assumption that the x distributions are the same for NC and CC. The hypothesis that the NC and CC data are the same distribution yields $\chi^2 = 8.2$ for 9 degrees of freedom, but $\chi^2 = 16.0$ if the CC data are scaled by the ratio of u_{vis} distributions of "flat" to $(1-y)^2$. The best fit to the linear combination $f(y) + f'(y) = 1 - \eta + 3\eta(1-y)^2$ yields $\eta = 0.08 \pm .21$ with $\chi^2 = 8.0$. In interpreting this result and the results

which follow it is important to recall that a cut in visible energy has been made and the neutral current acceptance depends on the y distribution. For a flat y distribution the acceptance is $A_L = .59$ and for a $(1-y)^2$ distribution it is $A_R = .37$. After correcting for the bias in acceptance: $f(y) + f'(y) = 3\eta'(1-y)^2 + (1-\eta')$ with $\eta' = .12 \pm .32$. The result should be compared with CITF (ref. 24), who obtain a result equivalent to $\eta' = .09 \pm .03$

4. <u>p and n cross-sections</u>

The total cross-sections on neutrons and protons separately can be thought of equivalently as measurements of the total cross-sections on u and d quarks. For CC the ratio of neutron to proton cross-sections ρ_{cc} is

$$\rho_{cc} = \frac{\sigma_{\nu n}}{\sigma_{\nu p}} = \frac{\int x[A_L\, u(x) + 1/3\, A_R\, \bar{d}(x)]\, dx}{\int x[A_L\, d(x) + 1/3\, A_R\, \bar{u}(x)]\, dx} \tag{48}$$

which follows from (14) and (19). For NC it is

$$
\begin{aligned}
\rho_{NC} = \int x dx \Bigg[& \left(A_L (C_V - C_A) + A_R \left(\frac{C_V + C_A}{3} \right) \right) u(x) \\
& + \left(A_L (C_V' - C_A') + A_R \left(\frac{C_V' + C_A'}{3} \right) \right) d(x) \\
& + \left(A_R \left(\frac{C_V - C_A}{3} \right) + A_L (C_V + C_A) \right) \bar{u}(x) + \left(A_R \left(\frac{C_V' - C_A'}{3} \right) + A_L (C_V' + C_A') \right) \bar{d}(x) \Bigg] \\
\Big/ \int x dx \Bigg[& \left(A_L (C_V - C_A) + A_R \left(\frac{C_V + C_A}{3} \right) \right) d(x) \\
& + \left(A_L (C_V' - C_A') + A_R \left(\frac{C_V' + C_A'}{3} \right) \right) u(x) \\
& + \left(A_R \left(\frac{C_V - C_A}{3} \right) + A_L (C_V + C_A) \right) \bar{d}(x) \\
& + \left(A_R \left(\frac{C_V' - C_A'}{3} \right) + A_L (C_V' + C_A') \right) \bar{u}(x) \Bigg]
\end{aligned}
\tag{49}
$$

which follows from (16) and (19). A_L and A_R are the acceptances for the flat y distribution and $(1-y)^2$ distribution as defined above.

The events with target neutrons are separated from events with target protons by looking at the event charge. The event charge is defined as the sum of the charges of the tracks at the primary vertex. In the absence of complications due to final state nuclear interactions, the neutron events would have charge 0 and the proton events would have charge 1. The nuclear effects of the neon nucleus, however, smear the expected charged distributions considerably. Most often the extra charge is positive indicating the presence of additional protons. Occasionally the extra charge is negative, indicating a proton that was too short to be visible. Other less important effects include π^- charge exchange close to the primary vertex and tracks measured so inaccurately that the sign of the charge is incorrect. Since extra protons are most often responsible for the extra charge, neglecting stopping protons when determining the event charge has the effect of shortening the long tail towards positive event charge while increasing slightly the number of events with negative charge. (A stopping proton is a positive particle whose track ends inside the bubble chamber without producing any visible decay products and whose length is consistent with the range of a proton of the measured momentum. If the track is short, the momentum is poorly measured, so short deuterons and α particles may meet the stopping proton definition). The charge distribution (without stopping protons) is given in figure 14. Two things are evident. First, the majority of events have charge 0 or 1. Second, NC are different from CC. It is qualitatively clear that the neutron cross-section is larger for CC than for NC. In order to be more quantitative,

however, it is necessary to understand the charge distribution.

No model which can be derived from first principles exists to describe the charge distribution. In lieu of such a model a phenomenological model is constructed. First some definitions: the probability that an event from a neon nucleus will have charge lower than the target particle is p_-. Similarly p_+ is the probability that the charge will be higher. It is assumed that p_+ and p_-, which depend only on interactions in or near the nucleus, are the same for both neutron and proton targets and for both NC and CC. The accuracy of the assumed equality of p_+ and p_- for neutron and proton targets depends on the details of the wave function for the neon nucleus. The equality of p_+ and p_- for NC and CC depends on their hadronic states being of the same multiplicity and energy. The CC have net charge +2 in the hadronic state while NC have net charge +1, but it is assumed that this difference is unimportant. The hydrogen in this mix presents a special case. It is expected that hydrogen events will rarely have a charge greater than 1 but that they will have charge 0 with probability f_H if the final state baryon is a stopping proton (which was eliminated before determining the charge). The relative numbers of neutrons, protons in neon, and protons in hydrogen are K_n, K_p, and K_H, which are numerically equal to .425, .417, and .158 respectively. The number of events from neutrons is given by

$$\text{neutrons} = \rho\, K_n\, T$$

where

$$T = N_T/(\rho\, K_n + K_p + K_H) \tag{50}$$

and N_T is the total number of events and ρ has the subscript NC or CC as appropriate. Similarly, the number of events from protons in neon is

$$\text{protons in Ne} = K_p\ T$$

and from protons in hydrogen it is

$$\text{protons in H} = K_H\ T$$

With the numbers of events from the various nuclei and the probabilities that the charge will be raised or lowered the charge distribution can be found. Let N_- be the number of events with negative charge. The events with negative charge are due to either neutron events with charge lowered or proton events with charge lowered by 2 or more. The latter is small as can be inferred from the small number of CC events (1.4%) with charge -2 or less. Neglecting the contribution of proton events the number of events with negative charge,

$$N_-/T = p_-\ \rho\ K_n \tag{51}$$

where p_- is the probability of lowering the charge and $\rho\ K_n\ T$ is the number of events with a neutron target. The number of events, N_0, with charge 0 is:

$$N_0/T = (1 - p_+ - p_-)\rho K_n + p_- K_p + f_H K_H \tag{52}$$

where $(1 - p_+ - p_-)$ is the probability that the charge is neither raised nor lowered, and f_H is the probability that a proton from a hydrogen event stops and thus is not counted in determining the charge. In (52) the coefficient of K_p should logically be the probability of lowering the charge by exactly 1, but that coefficient is nearly equal to p_- since the probability of lowering the charge by more than 1 is small. Similarly

$$N_+/T = f_n \rho K_n + (1 - p_+ - p_-) K_p + (1 - f_H) K_H \tag{53}$$

$$N_{++}/T = p_+ K_p + (p_+ - f_n)\rho K_n \tag{54}$$

where N_+ and N_{++} are the number of events with charge +1, and more than +1, respectively, and f_n is the probability of raising the charge of a neutron event by exactly one. If (51)-(54) are used for $\rho = \rho_{NC}$ and also for $\rho = \rho_{CC}$ with the same p_+, p_-, f_n and f_H, a total of 8 equations with 6 unknowns is obtained. Furthermore, it has been determined from a similar experiment in hydrogen that $f_H = 0.07$.[27] Since the energy loss in the hydrogen-neon mix is 2.7 times the energy loss in pure hydrogen, more protons will stop in the mix. A Monte Carlo estimate, which depends on the proton spectrum yields $f_H = .09$. However, the results are not sensitive to the value of f_H.

A series of fits to the data has been performed with the parametrization (51) - (54) with p_-, p_+, ρ_{CC}, and ρ_{NC} parameters of the fit and f_H and f_n held constant. The value of f_n is varied in the fits as shown in Table VIa. As can be seen, acceptable fits with a wide

variety of ρ_{CC} and ρ_{NC} may be obtained depending on the assumed value of f_n. To reduce the error on ρ_{NC}, ρ_{CC} is held fixed at 1.9 in the fits in Table VIb. The value $\rho_{CC} = 1.9$ can be obtained from the x distributions of Field and Feynman (ref. 24). The ratio of neutron to proton cross-sections for neutral currents is then $\rho_{NC} = 1.27 \pm .36$. The last two fits vary f_H showing that the result is not sensitive to small variations in f_H. No high energy neutrino experiment has determined ρ_{CC} although $\rho_{CC} = 1.9$ is consistent with a deuterium bubble chamber experiment at $E_\nu \cong 4$ GeV.[28] Hung and Sakurai[29], however, give ρ_{NC} for several models based on $\rho_{CC} = 1.56$. In view of the uncertainty of the correct value for ρ_{CC} Table VIc presents the result of several fits for various assumed values of ρ_{CC}. In all these fits the ratio of ρ_{NC}/ρ_{CC} is approximately constant and is equal to 0.7 ± 0.2. The final two columns in Table VIc give R_ν^p and R_ν^n, the predicted neutral rates (NC/CC) for purely proton and neutron targets respectively.

5. z_{yis} distribution

The quark fragmentation functions $D_q^h(z)$ provide a means of probing the neutral current if the functions are known. In CC (see eqn. 21) $D_u^h(z)$ is just the multiplicity of hadron type h at $z_i = E_i/\nu$, where E_i is the hadron energy and ν is the energy transferred to the hadron system. Thus the charged current data determine $D_u^h(z)$.

Experimentally there are two problems. First, the type of hadron (π, K, p, etc.) is not generally known. Second, z is not measured but rather the particle momentum and some estimate of the hadronic energy based on the charged particles only. Therefore, a variable z_{vis} is defined:

$$(z_{vis})_i = p_i/E_h \tag{55}$$

The D functions exhibit a singularity (1/z) as $z \to 0$, so it is more convenient to work with $z\, D_q^h(z)$ instead. The multiplicity, N(z), weighted by z is shown in figure 15 for positives and negatives from charged current interactions. The curves shown are $zD_u^{\pi^+}(z)$ for positives and $zD_u^{\pi^-}(z)$ for negatives and are normalized to the data for $z_{vis} > 0.2$, where the fragmentation functions are expected to be valid. There is only one normalization constant for both positives and negatives; the relative magnitudes of $D_u^{\pi^+}(z)$ and $D_u^{\pi^-}(z)$ are significant. The parameterization of $D_u^{\pi^+}(z)$ and $D_u^{\pi^-}(z)$ is due to Field and Feynman (ref. 24). For $z_{vis} > 0.2$ the χ^2 is 12.3 for 15 degrees of freedom. The ratio of positives to negatives is 2.3 ± 0.3 for $.2 < z_{vis} < .6$ but increases to $5.0^{+5}_{-2.5}$ for $z_{vis} > .6$ and for $z_{vis} > 0.7$ is greater than 8.0 at 68% confidence level. The increase in the ratio of positives to negatives as $z_{vis} \to 1$ can be understood in terms of the quark fragmentation picture. The u quark emerging from a neutrino interaction will fragment into:

$$u \rightarrow (u\bar{d}) + d = \pi^+ + d$$

or

$$u \rightarrow (u\bar{u}) + u = (\pi^\circ, n) + u$$

but not:

$$u \rightarrow \pi^- + \text{quark}.$$

Since the leading particles come from the fragmentation of the initial quark the large positive to negative ratio observed is explained. However, the large positive to negative ratio is also easily explained by charge conservation and the fact that a limited amount of energy is available to the hadron system. In any given event the sum of the z's of all the hadrons must equal one. Therefore, if one hadron is at $z \cong 1$ then the other hadrons must be near $z \cong 0$, and, unless the energy is very large, there cannot be too many hadrons. Since the overall hadron state charge is +1 (struck neutron) or +2 (struck proton) the leading particle at $z \cong 1$ will be positive much more often than negative - just from charge conservation.

In the following, however, the quark fragmentation picture will be considered valid and therefore a useful probe of the neutral current. In NC the positive hadrons will come from the fragmentation of both u and d quarks. The multiplicity of positives (N^+) is of the form

$$N^+(z) \propto (1-\lambda)\, D_u^{\pi^+}(z) + \lambda\, D_d^{\pi^+}(z)$$

and for negatives

$$N^-(z) \alpha (1-\lambda) D_u^{\pi^-} + \lambda D_d^{\pi^-}(z)$$

where λ is a parameter describing the relative strengths of u and d quarks in NC (compare with eqn. 25). The data for neutral currents are shown in figure 16. The best fit to the parameter λ is $\lambda = 0.56 \pm 0.10$ and the χ^2 for the fit is 24.6 for 14 degrees of freedom. The curves for the best fit are also shown on figure 16. Neither the positives nor the negatives follow the predicted curves particularly well, but more accurate data are needed to judge whether the quark fragmentation model describes the leading hadrons in NC. The corresponding value of λ for a target with equal numbers of protons and neutrons is calculated to be 0.58 ± 0.10 using the x distributions of Field.

A less model dependent approach to the data may be taken. The data show evidence for leading negatives in NC. For $z_{vis} > 0.6$ the ratio of positives to negatives is $0.1 \begin{smallmatrix} +0.4 \\ -0.1 \end{smallmatrix}$. Any difference between the π^+ and π^- distribution in z in NC from an isoscalar target requires that the neutral current has both I = 1 and I = 0 components of I-spin. In this case, the target is not isoscalar (15% hydrogen), and the particles are not known to be π's. However, neither the excess of hydrogen nor the contamination of other particles (K,p) provides an easy explanation for leading negatives.

Transverse Momentum

The transverse momentum distribution in CC and NC is given in figure 17. The transverse momentum is the momentum of each hadron perpendicular to the momentum vector of the observed hadronic particles. The fall with transverse momentum seems to be nearly the same in CC and NC. The hypothesis that CC and NC come from the same distributions yields $\chi^2 = 18.9$ for 17 degrees of freedom.

VI. CONCLUSION

Neutral current events have been observed at a rate 0.35 ± 0.06 of the charged current rate for $E_h > 10$ GeV. This measurement confirms the now well established existence of the weak neutral current. The distribution of NC in a new variable u_{vis}, which depends on both x and y, has been presented. From this distribution it has been concluded that for a neutral current y distribution of the form $1-\eta + 3\eta\ (1-y)^2$ $\eta = 0.12 \pm 0.32$. The result is consistent with but less precise than the CITF result $\eta = 0.09 \pm 0.03$, which was obtained by a different method. The results that depend on measuring the charge and momenta of the particles in the hadronic state are a new contribution to the study of the neutral current. It has been shown that the ratio of the ratio of neutron to proton cross sections in NC to that in CC is 0.7 ± 0.2. A model dependent fit to the z_{vis} distribution with the quark-π fragmentation functions $D_q^{\pi}(z)$ yields a best fit with the fractional strength of d quarks, $\lambda = .56 \pm .10$. These two results suggest that the u and d quarks couple to the neutral current with approximately equal strengths.

APPENDIX

To determine the number of muons in a sample of leaving tracks, the formalism developed in ref. 9 is used. For every track passing through the EMI a confidence level C_μ for a muon hypothesis and a confidence level C_h for a hadron hypothesis are defined. C_μ is the probability that a muon would have a worse match between the extrapolated position and the position measured in the proportional chamber, and C_h is the probability that a hadron would have a better match. C_μ is a function of:

1) The χ^2 of the match between the extrapolated position measured in the proportional chamber.
2) The predicted horizontal and vertical errors (σ_x and σ_y)
3) The density of background hits in the EMI (ρ_c)
4) The proportion chamber inefficiency (ε_c)
5) The angle of the match $\tan \beta = (\Delta_y \sigma_x)/(\Delta_x \sigma_y)$ where Δ_x and Δ_y are the horizontal and vertical differences between extrapolated and measured positions.

C_h is a function of all of the above and also the number of absorption lengths in the absorber (ℓ/λ). The dependence of C_μ and C_h on these variables is below, but a knowledge of explicit formulas for C_μ and C_h will not be required for what follows.

$$C_\mu = \left[(1-\varepsilon_c)\left((1-\delta)\exp(-\frac{\chi^2}{2})\right.\right. \tag{1}$$

$$\left.\left. + \delta \exp(-\frac{1}{2}(\frac{\Delta x^2}{\sigma_x'^2} + \frac{\Delta y^2}{\sigma_y'^2}))\right) + \varepsilon_c\right] \exp(-\pi\sigma_x\sigma_y\rho\ \chi^2)$$

$$1-C_h = (1-e^{-\ell/\lambda})\exp(-\pi\sigma_x\sigma_y\rho_c\chi^2) \tag{2}$$

$$+ e^{-\ell/\lambda}\ C_\mu$$

where

$$\chi^2 = \frac{\Delta x^2}{\sigma_x^2} + \frac{\Delta y^2}{\sigma_y^2} \tag{3}$$

and

$$\sigma_x'^2 = \sigma_x^2 + \xi^2$$

$$\sigma_y'^2 = \sigma_y^2 + \xi^2 \tag{4}$$

and ξ and δ are constants whose values are given in reference 9 as $\xi = 1.7$ cm and $\delta = 0.1$. To simplify the notation, the set of parameters (except χ^2) on which C_μ and C_h depend will be labeled as α. Thus

$$C_\mu = C_\mu(\chi^2, \alpha) \tag{5}$$

$$C_h = C_h(\chi^2, \alpha). \tag{6}$$

For fixed α (1) and (2) define a set of parametric equations and, in principle, χ^2 may be eliminated. In what follows C_μ will be considered to be the independent variable and C_h a dependent variable

$$C_h = C_h'\ (C_\mu, \alpha). \tag{7}$$

The right hand side carries a prime to emphasize that the functional form is different from that in (2), but in what follows the prime will be dropped to simplify notation. To begin, α is taken to be fixed. Since no two tracks will have precisely the same α, it will be necessary to sum over all possible α later. It is an important feature of the method that an explicit expression for the estimator is derived and that the summation over α is therefore possible.

The parametric equations for fixed α define a curve in the C_μ-C_h plane. Each muon with the given α will occur at some point along the curve. Some typical curves are shown in figure 18. A statistical ensemble of muons will populate the curve such that the density of points is uniform when projected on the C_μ axis. Similarly a statistical ensemble of hadrons will populate the curve such that the density of points is uniform when projected on the C_h axis.

The distribution of muons in C_h is

$$L = -\left(\frac{\partial C_\mu}{\partial C_h}\right)_\alpha . \tag{8}$$

Equation 8 follows from the fact that the distribution of muons is uniform in C_μ and that the derivative (8) transforms distributions in C_μ to distributions in C_h.

The geometric interpretation of L is that it is the absolute value of the inverse of the slope of the curve on figure 18. L depends on the set of parameters α; figure 18 shows the variation of the curves with one parameter in the set α, namely ρ_c. The curve $\rho_c = 2$ is a typical curve for muons with a momentum of about 5 GeV/c. For this curve L is large

for most muons (95% of the muons will occur above $C_\mu = 0.05$ where $L = -\left(\frac{\partial C_\mu}{\partial C_h}\right)_\alpha$ is large). Similarly L is small for most hadrons (95% of the hadrons will have $C_h > 0.05$ where L is small). However, L is large for some hadrons and small for some muons. This situation is merely a reflection of the fact that the hadron-muon separation is not perfect in the EMI. As ρ_c, the number of background hits, becomes larger, the hadron-muon separation becomes worse. The lack of separation is seen geometrically in figure 18 where L approaches a constant equal to 1 independent of C_μ as $\rho_c \to \infty$.

To count the number of muons in a sample of tracks passing through the EMI, a function $G(C_\mu,\alpha)$ is defined such that G, on the average, has some value for muons and another average value for hadrons. Such a function could be L itself. Another function (the one which was eventually chosen for this work) is

$$G = \frac{L}{L+1} . \tag{9}$$

This function has the property that it is ≈ 1 for most muons and ≈ 0 for most hadrons.

Consider the muon estimate

$$N_\mu = \sum_{i=1}^{N} \phi_i = \sum_{i=1}^{N} \frac{G_i - \langle G \rangle_h}{\langle G \rangle_\mu - \langle G \rangle_h} \tag{10}$$

where N is the number of tracks in the sample and $\langle G \rangle_\mu$ and $\langle G \rangle_h$ are the average values of G for muons and hadrons respectively. Equation 10 serves as the definition of ϕ_i and N_μ. If the sample contains only muons,

then the average value of N_μ is

$$\langle N_\mu \rangle_{muons} = N \frac{\langle G \rangle_\mu - \langle G \rangle_h}{\langle G \rangle_\mu - \langle G \rangle_h} = N . \tag{11}$$

If the sample contains only hadrons then the average value of N_μ is

$$\langle N_\mu \rangle_{hadrons} = N \frac{\langle G \rangle_h - \langle G \rangle_h}{\langle G \rangle_\mu - \langle G \rangle_h} = 0. \tag{12}$$

Since any subsample can be considered as the sum of a sample that consists only of muons and a sample that consists only of hadrons, N_μ is an unbiased estimate of the number of muons in any sample with fixed α. If there is a sample with different values of α, an estimate $N_\mu(\alpha)$ can be found for each value of α. The muon estimate, N_μ is just the sum of the $N_\mu(\alpha)$. However, this procedure is identical to applying (10) without restriction on α. Thus N_μ is an unbiased estimate of the number of muons in any sample.

The average values of G for muons and for hadrons are

$$\langle G \rangle_\mu = \int_0^1 G(C_\mu, \alpha) \, d\, C_\mu \tag{13}$$

and

$$\langle G \rangle_h = \int_0^1 G(C_\mu,\alpha)\ d\ C_h$$

$$= \int_0^1 G(C_\mu,\alpha) \left| \left(\frac{\partial\ C_h}{\partial\ C_\mu} \right) \right|\ d\ C_\mu \tag{14}$$

$$= \int_0^1 \frac{G(C_\mu,\alpha)}{L}\ d\ C_\mu .$$

The error in N_μ can be estimated by defining f_μ by

$$N_\mu = f_\mu N \tag{15}$$

The error in N_μ is then

$$(\delta N_\mu)^2 = N^2(\delta f_\mu)^2 + f_\mu{}^2(\delta N)^2 \tag{16}$$

since f_μ and N are statistically independent. If N is not too small:

$$(\delta N)^2 = N \tag{17}$$

and

$$(\delta f_\mu)^2 = (\overline{\phi^2} - \overline{\phi}^2)/N \tag{18}$$

where

$$\overline{\phi^2} = \frac{1}{N}\sum_{i=1}^{N} \phi_i^2 \tag{19}$$

substituting (17) and (18) into (16) the result

$$(\delta N_\mu)^2 = N\ \overline{\phi^2} \tag{20}$$

is obtained. Equations (10) and (20) constitute an estimate of the number of muons and error in the number of muons.

For this work G was chosen to be the function (9). Any choice of G will give an unbiased estimate of the number of muons, N_μ, except, of course, that functions for which $\langle G \rangle_\mu = \langle G \rangle_h$ are not allowed. However, some functions will result in larger statistical errors (eqn 20) than other functions. The particular choice for G was made from the results of comparing the relative sizes of the statistical errors for several choices of G. It is not known whether some better choice of the function G might have been made.

Test of the Method

A sample of muons was obtained by selecting a sample of noninteracting tracks passing through the bubble chamber. After requiring the track momentum to be greater than 10 GeV/c and within 2.5° of the beam direction in both dip and azimuth, a sample of 450 tracks was obtained. With these kinematic cuts the sample was known to consist of $99.5 \pm 0.5\%$ muons. The statistical estimate of the number of muons in the sample was 444 ± 9 ($99 \pm 2\%$ muons).

A sample of hadrons was obtained from CC after removing the identified muon. The sample of 461 tracks contained $99 \pm 1\%$ hadrons. The statistical estimate of the number of muons in the sample was 7 ± 13 ($98 \pm 3\%$ hadrons).

REFERENCES

1. A. R. Clark, et. al., Phys. Rev. Lett., 26 (1971) 1667. and W. C. Carithers, et. al., Phys. Rev. Lett. 30 (1973) 1336.
2. F. J. Hasert, et. al., Phys. Lett. B46 (1973) 138 and A. Benvenuti, et. al., Phys. Rev. Lett. 32 (1974) 800.
3. F. Reines, et. al., Phys. Rev. Lett. 37 (1976) 315.
   D. Cline, et. al., Phys. Rev. Lett. 37 (1976) 252.
   S. J. Barish, et. al., Phys. Rev. Lett. 33 (1974) 448.
   D. Cline, et. al., Phys. Rev. Lett. 37 (1976) 648.
   W. Lee, et. al., Phys. Rev. Lett. 37 (1976) 186.
   S. J. Barish, et. al., Phys. Rev. Lett. 34 (1975) 538.
4. See, for example, A. De Rújula, et. al., Rev. Mod. Phys. 46 (1974) 391 and references contained therein.
5. J. von Krogh, et. al., Phys. Rev. Lett. 36 (1976) 710. and P. B. Bosetti, et. al., Phys. Rev. Lett. 38 (1977) 1248.
6. F. A. Nezrick, IEEE Trans. on Nucl. Sci. NS-22 (1975) 1479.
7. Fermi National Accelerator Laboratory 15-foot Bubble Chamber Safety Report, edited by R. R. Huson, 1972 (unpublished), Vols. I-III.
8. It may be confusing that a fifteen foot bubble chamber should have a diameter of somewhat less than 4 meters. However, the distance from the tip of the "snout" or hadron beam entrance (see figure 2) to the back of the chamber is about 4.6 meters or 15 feet.
9. R. J. Cence, et. al., Nucl. Inst. and Meth. 138 (1976) 245.
10. F. T. Solmitz, et. al., Group A Programming Note P-117, Lawrence Berkeley Laboratory, 1966 (unpublished).

11. B. Pardoe and M. Leavitt, Group A Programming Note P-235, Lawrence Berkeley Laboratory, 1974 (unpublished).

12. O. I. Dahl, et al., Group A Programming Note P-126, Lawrence Berkeley Laboratory, 1968 (unpublished).

13. V. Barger, et al., report COO-574, University of Wisconsin, 1976 unpublished.

14. The Monte Carlo is a slightly modified version of the one developed by W. G. Scott and collaborators at Fermilab.

15. V. Barger, Nucl. Phys. B102 (1976) 439.

16. O. Czyzerski and K. Rybicki, Proc. 15th International Conference on High Energy Physics, Kiev, 1970, p. 689.

17. J. W. Chapman, et. al, Phys. Rev. Lett. 36 (1976) 124.

18. L. Van Hove, Nucl. Phys. B9 (1969) 331.

19. G. Myatt, ECFA 300 GeV Working Group report (unpublished), Vol. II, p. 177. See also J. W. Chapman, et. al., Phys. Rev. D 14 (1976) 5.

20. The "μ decay" in Table I is considered to be a hadron signature since it is more likely to be a π decay with the μ unobserved than a μ decay. The distributions are, however, corrected for stopping μ's which are misidentified as hadrons by this interpretation.

21. R. J. Loveless, et. al., (to be published).

22. The likelihood ratio is defined as $L = -\frac{\partial Cu}{\partial C_h}$. Explicit expressions for C_μ and C_h are given in Ref. 9 where they are referred to as P_μ and P_h respectively. See Appendix also.

23. A. Benvenuti, et. al., Phys. Rev. Lett. 37 (1976) 1039.

24. R. D. Field and R. P. Feynman, Phys. Rev. D 15 (1977) 2590.

25. W. von Donink, Aachen Neutrino Conference, 1976 (unpublished).

26. L. Stutte, Proceedings of the International Conference on Production of New Particles with New Quantum Numbers, Madison, Wisconsin, 1976, edited by D. B. Cline and J. J. Kolonko (University of Wisconsin, Madison, 1976), p. 388.

27. G. R. Lynch, private communication.

28. S. J. Barish, et. al., Physics Letters 66B (1977) 291.

29. P. Q. Hung and J.J. Sakurai, Physics Letters 63 B (1976) 295.

30. M. Holder, et. al., "Measurement of the Neutral to Charged Current Cross Section Ratio in Neutrino and Antineutrino Interactions", Preprint.

Work performed under the auspices of the U. S.
Energy Research and Development Administration.

TABLE I

TRACK LABELS

Label	Meaning
Interaction	Track produces a hadronic interaction
Ending	Endpoint within the bubble chamber. Could be a stopping proton or π^-, K^- charge exchange
Electron	Electron identified by spiralization or bremsstrahlung losses
π decay	π decay at rest followed by a μ decay
μ decay	μ decay rest or π decay with the μ not visible
Leaving	None of the above labels apply

TABLE II

SUMMARY OF MEASURED EVENTS ELIMINATED BY PRELIMINARY CUTS

Unmeasurable Events	670
Geometry Program (TVGP) failures	1255
$\Sigma P_x < 1$ GeV/c	4102
Outside fiducial volume	470
EMI not working	120
Selected for further analysis	3276
Total number of events	9893

TABLE III

SUMMARY OF NC CUTS

Cut Intended to Eliminate	Events Eliminated E_{vis}>5 GeV in ( )	Fraction of Specific Background Eliminated	Fraction of NC Lost
1) Electron Neutrino	9 (8)	.40	.000
2) Charged Hadron Interactions	22 (14)	.80	.001
3) Muon anti-neutrino	37 (35)	.85	.012
4) K°, Λ decays	268 (50)	.99	.01
5) CC - high transverse momentum negative interacts	2017 (1736)	.95	.51
Remaining neutral current candidates	923 (280)		

TABLE IV

NC BACKGROUND SUBTRACTION

E_{vis}(GeV)	N	N_μ	N_A	CC(p_μ>3GeV/c)	N'_u	N_ν	CC(p_μ<3GeV/c)	NC (r=.6)	NC (r=.5)	NC (r=.7)
5-10	278.9	189.1	89.8	-2.2	186.9	152.4	-9.3	143.1	112.1	163.9
10-15	113.3	93.3	20.0	-6.4	86.9	88.3	-10.3	78.0	73.3	81.1
15-20	66.9	57.8	9.1	-1.2	56.6	60.6	-6.6	54.0	52.8	54.9
20-30	45.9	43.2	2.7	-6.7	36.5	37.8	-8.5	29.4	29.1	29.6
30-50	37.7	32.8	4.9	-3.6	29.2	28.3	-5.0	23.3	22.0	24.2
50-90	24.4	24.4	0	-1.9	22.5	24.5	-1.5	23.0	23.5	22.7

0 0 0 0 4 8 0 1 9 3 4

TABLE V. Comparison of Neutral Current Rates from Various Experiments

Experiment	Rate	Comment
Gargamelle (ref.25)	0.28±0.04	CERN heavy liquid bubble chamber $\langle E_\nu \rangle \sim 2$ GeV $E_h > 1$ GeV
HPWF (ref.23)	0.29±0.04	FNAL counter $\langle E_\nu \rangle \sim 50$ GeV, E_h 4GeV
CITF (ref.26)	0.28±0.03	FNAL counter $\langle E_\nu \rangle \sim 50$ GeV, E_h 12 GeV
CDHSB (ref.30)	0.293±0.010	CERN counter $\langle E_\nu \rangle \sim 110$GeV, $E_h > 12$ GeV
This experiment	0.35±0.06	FNAL H-Ne bubble chamber $\langle E_\nu \rangle \sim 35$ GeV, $E_h > 10$ GeV

TABLE VI. Fitted ratio of neutron to proton cross sections

	ρ_{CC}	ρ_{NC}	P_+	P_-	f_n	f_H	χ^2	R_ν^P	R_ν^{n**}
a)	1.36±0.17	1.02±0.26	0.19±0.02	0.12±0.02	0.05*	0.09*	5.07		
	1.51±0.20	1.09±0.29	0.22±0.02	0.12±0.02	0.10*	0.09*	4.84		
	1.72±0.25	1.18±0.32	0.25±0.02	0.11±0.02	0.15*	0.09*	4.59		
	2.02±0.33	1.31±0.38	0.29±0.02	0.11±0.02	0.20*	0.09*	4.29		
	3.36±0.87	1.81±0.61	0.38±0.02	0.09±0.1	0.30*	0.09*	3.66		
b)	1.90*	1.27±0.36	0.28±0.03	0.11±0.01	0.19±0.05	0.09*	4.38		
	1.90*	1.28±0.36	0.27±0.03	0.11±0.01	0.18±0.05	0.05*	4.37		
	1.90*	1.25±0.37	0.29±0.03	0.11±0.01	0.21±0.05	0.15*	4.40		
c)	1.30*	1.00±0.25	0.18±0.04	0.13±0.02	0.04±0.07	0.09*	5.14	.39±.08	.30±.07
	1.40*	1.04±0.27	0.20±0.04	0.12±0.02	0.07±0.06	0.09*	4.99	.40±.08	.30±.07
	1.50*	1.09±0.29	0.22±0.04	0.12±0.02	0.10±0.06	0.09*	4.48	.41±.09	.30±.07
	1.60*	1.13±0.31	0.24±0.04	0.12±0.02	0.13±0.06	0.09*	4.71	.41±.09	.30±.07
	1.70*	1.18±0.33	0.25±0.04	0.11±0.02	0.15±0.05	0.09*	4.58	.42±.09	.29±.07
	1.80*	1.22±0.35	0.27±0.04	0.11±0.01	0.17±0.05	0.09*	4.48	.43±.09	.29±.07
	1.90*	1.27±0.37	0.28±0.03	0.11±0.01	0.19±0.05	0.09*	4.38	.43±.09	.29±.07
	2.00*	1.31±0.38	0.29±0.03	0.11±0.01	0.20±0.05	0.09*	4.29	.44±.09	.29±.07

*Held fixed during fit

**These numbers use the value $R_\nu = 0.35 \pm 0.6$ measured in this experiment. More precise numbers can be obtained using more precise values of R_ν as measured by other experiments.

FIGURE CAPTIONS

Fig. 1 Neutrino CC energy spectrum.

Fig. 2 Plan and elevation views of the 15-ft. bubble chamber and EMI. The proportional chambers are mounted directly on the vacuum tank to maximize solid angle coverage. The magnet coils and zinc inside the vacuum tank constitute the hadron absorber.

Fig. 3. Distribution of CC in visible energy. The curve is the Monte Carlo prediction.

Fig. 4. Distribution of CC in $y_{vis} = (E_{vis} - p_\mu)/E_{vis}$. The solid curve "flat" is the distribution predicted by the Monte Carlo for a distribution which is flat in y. The solid curve "$(1-y)^2$" is the distribution predicted by the Monte Carlo for a distribution proportional to $(1-y)^2$. The dashed curve is a fit to a linear combination of the two solid curves for the y distribution $1 - \varepsilon + 3\varepsilon\,(1-y)^2$ with $\varepsilon = 0.16 \pm 0.04$.

Fig. 5 Distribution of CC in $v = xy$. The curve is the Monte Carlo prediction.

Fig. 6 Distribution of CC in transverse muon momentum with respect to the neutrino beam.

Fig. 7 The probability that a hadron will be identified by an interaction or decay in the bubble chamber as a function of its momentum p.

Fig. 8 Distribution of the NC candidates in visible energy. The shaded events are associated with other events seen in the chamber or on the wall.

Fig. 9 The fraction of CC which appear to be associated as a function of visible energy.

Fig. 10 Distribution of CC and NC in visible hadronic energy.

Fig. 11 Ratio of NC to CC as a function of visible hadronic energy. Curves are shown for the energy dependence for the ratio if the NC have a y distribution which is flat or, alternatively, a y distribution proportional to $(1-y)^2$.

Fig. 12 Distribution of CC and NC in event transverse momentum balance (P_T).

Fig. 13 Distribution of NC and CC in $u_{vis} = E_h \sin^2\theta_h/2Mp$. The curve labeled "flat" is a smooth curve drawn through the CC data and normalized to the NC data. The durve labeled "$(1-y)^2$" is the "flat" curve scaled by the ratio of the Monte Carlo predictions for $(1-y)^2$ to flat y distributions. The best fit $f(y) + f'(y) = (1-\eta) + 3\eta(1-y)^2$ with $\eta = 0.12 \pm 0.32$ was obtained directly from the data points and did not make use of the curves.

Fig. 14 Distribution of NC and CC in event charge with stopping protons excluded.

Fig. 15 Distribution in z_{vis} of positive and negative tracks for CC, where $z_{vis} = p_i/E_h$ and p_i is the momentum of the hadron. $N(z_{vis})$ is the number of positive or negative hadrons. Upper limits (68% confidence level) are given for points below the z_{vis} axis. The curves are $D_u^{\pi^+}(z)$ and $D_u^{\pi^-}(z)$ from Field and Feynman (ref. 24) and are normalized to the data for $z_{vis} > 0.2$.

Fig. 16 Distribution in z_{vis} of positive and negative tracks for NC. Upper limits (68% confidence level) are given for points below

the z_{vis} axis. The curves are the linear combinations $(1-\lambda)D_u^{\pi+}(z) + \lambda D_u^{\pi-}(z)$ and $\lambda D_u^{\pi+}(z) + (1-\lambda) D_u^{\pi-}(z)$ with $\lambda = 0.56 \pm .10$ normalized to the data for $z_{vis} > 0.2$.

Fig. 17 Distribution hadron transverse momentum in NC and CC. The transverse momentum is taken with respect to the sum of the momenta of the visible hadronic particles.

Fig. 18 Typical curves of C_h vrs C_μ.

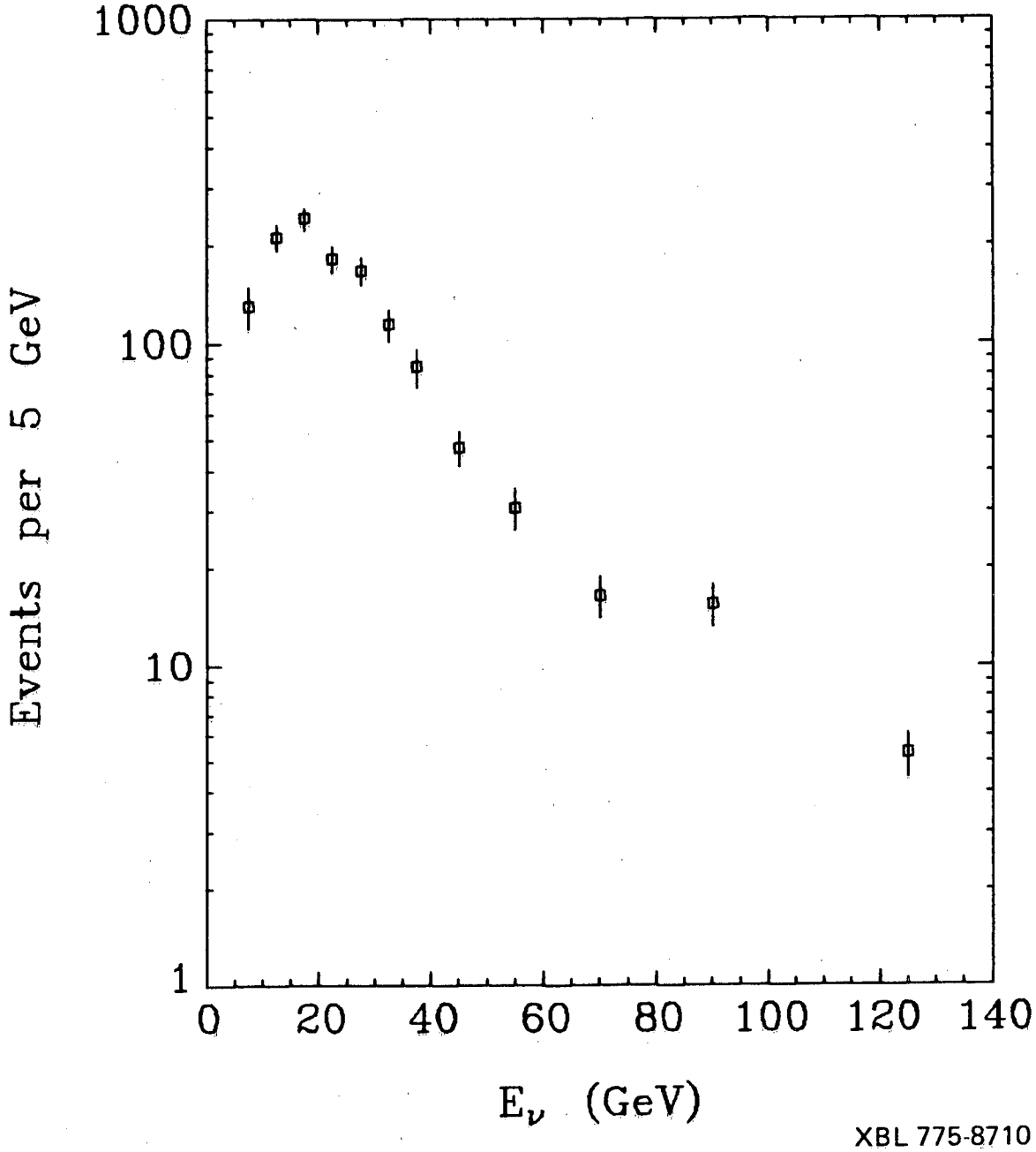

XBL 775-8710

Figure 1

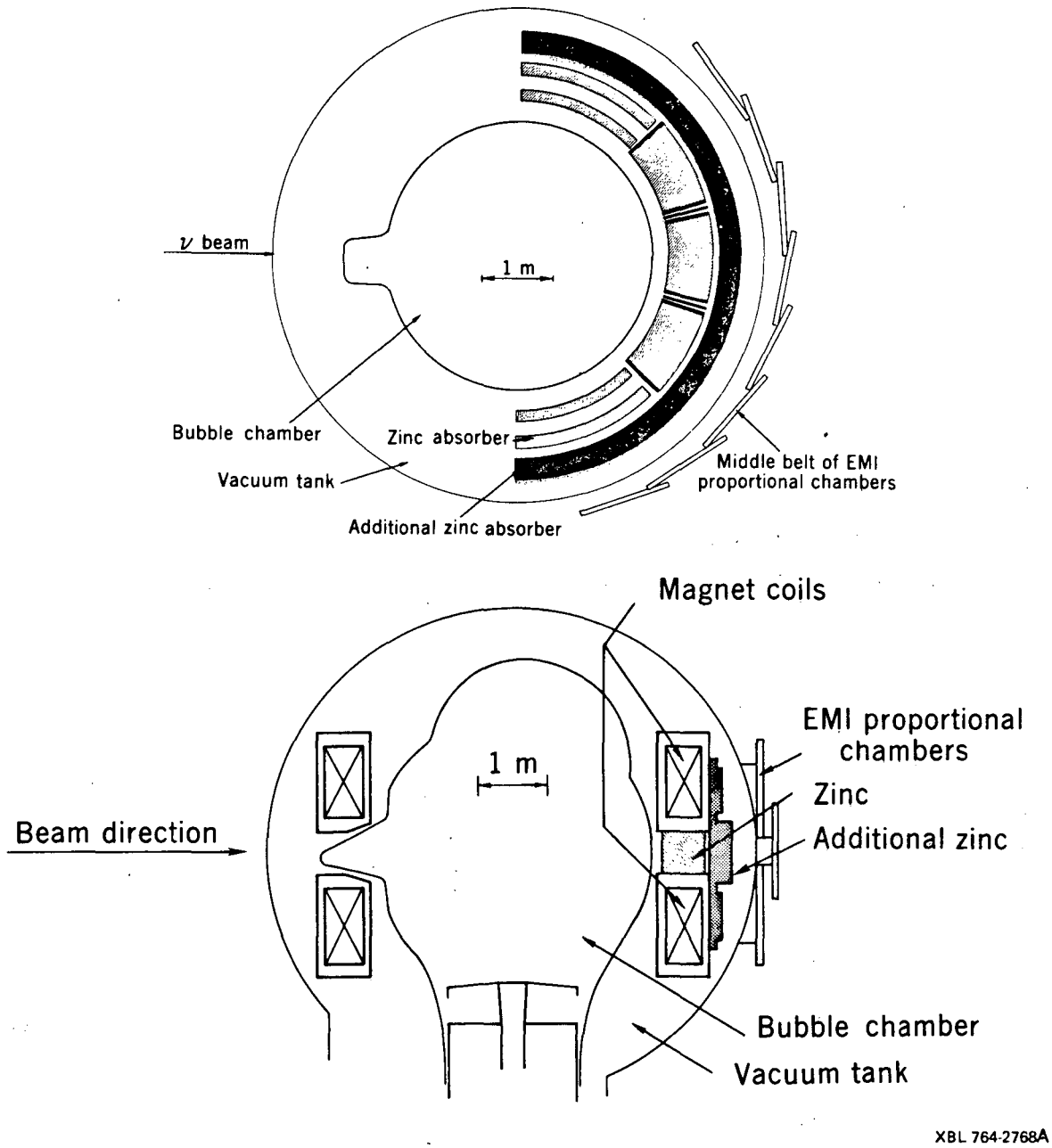
ν beam
1 m
Bubble chamber
Zinc absorber
Vacuum tank
Additional zinc absorber
Middle belt of EMI proportional chambers
Magnet coils
EMI proportional chambers
Zinc
Additional zinc
1 m
Beam direction
Bubble chamber
Vacuum tank
XBL 764-2768A

Figure 2

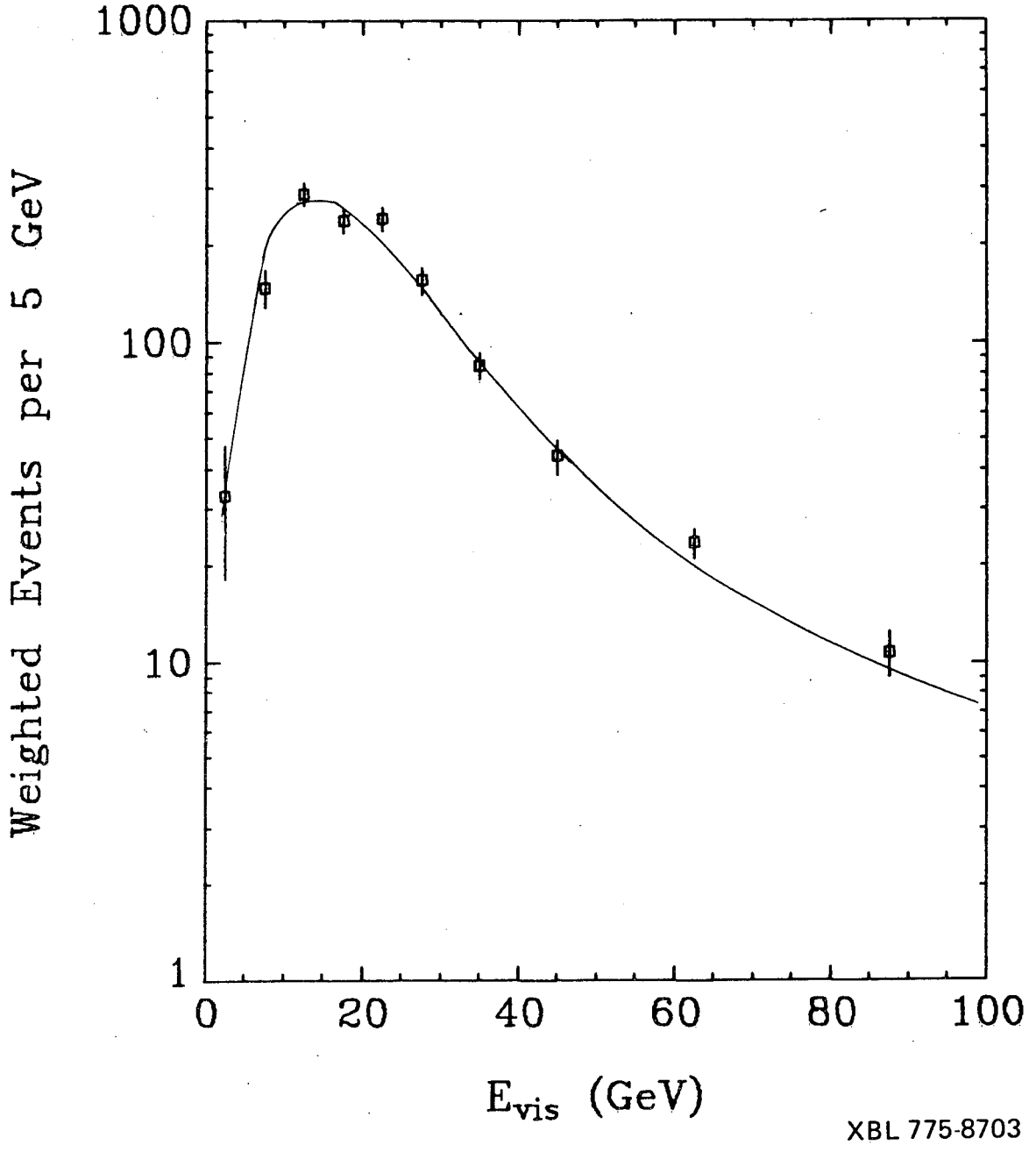
1000
100
10
1
Weighted Events per 5 GeV
0
20
40
60
80
100
E_{vis} (GeV)
XBL 775-8703

Figure 3

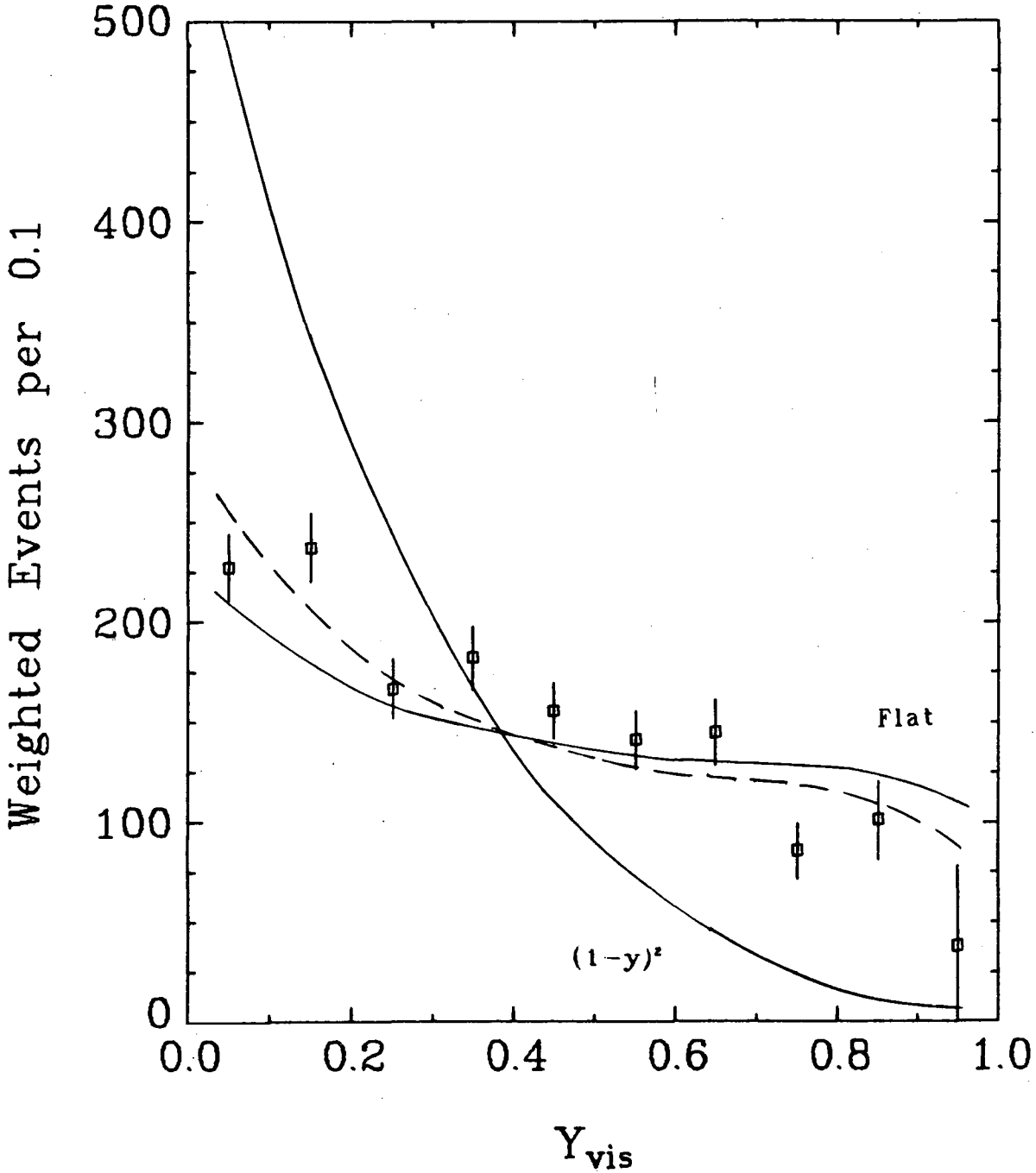

XBL 776-9059

Figure 4

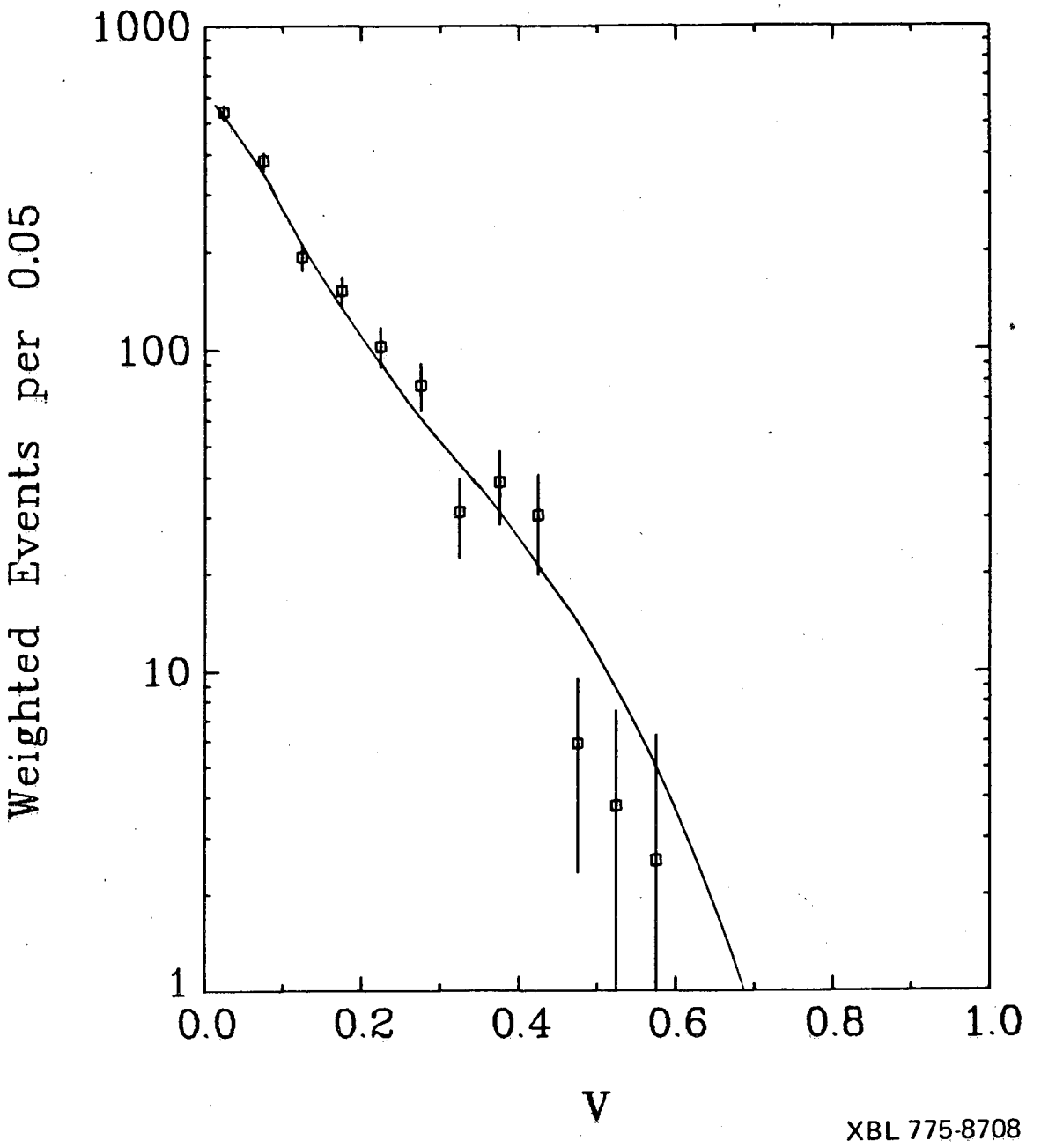
1000
100
10
1
Weighted Events per 0.05
0.0
0.2
0.4
0.6
0.8
1.0
V
XBL 775-8708

Figure 5

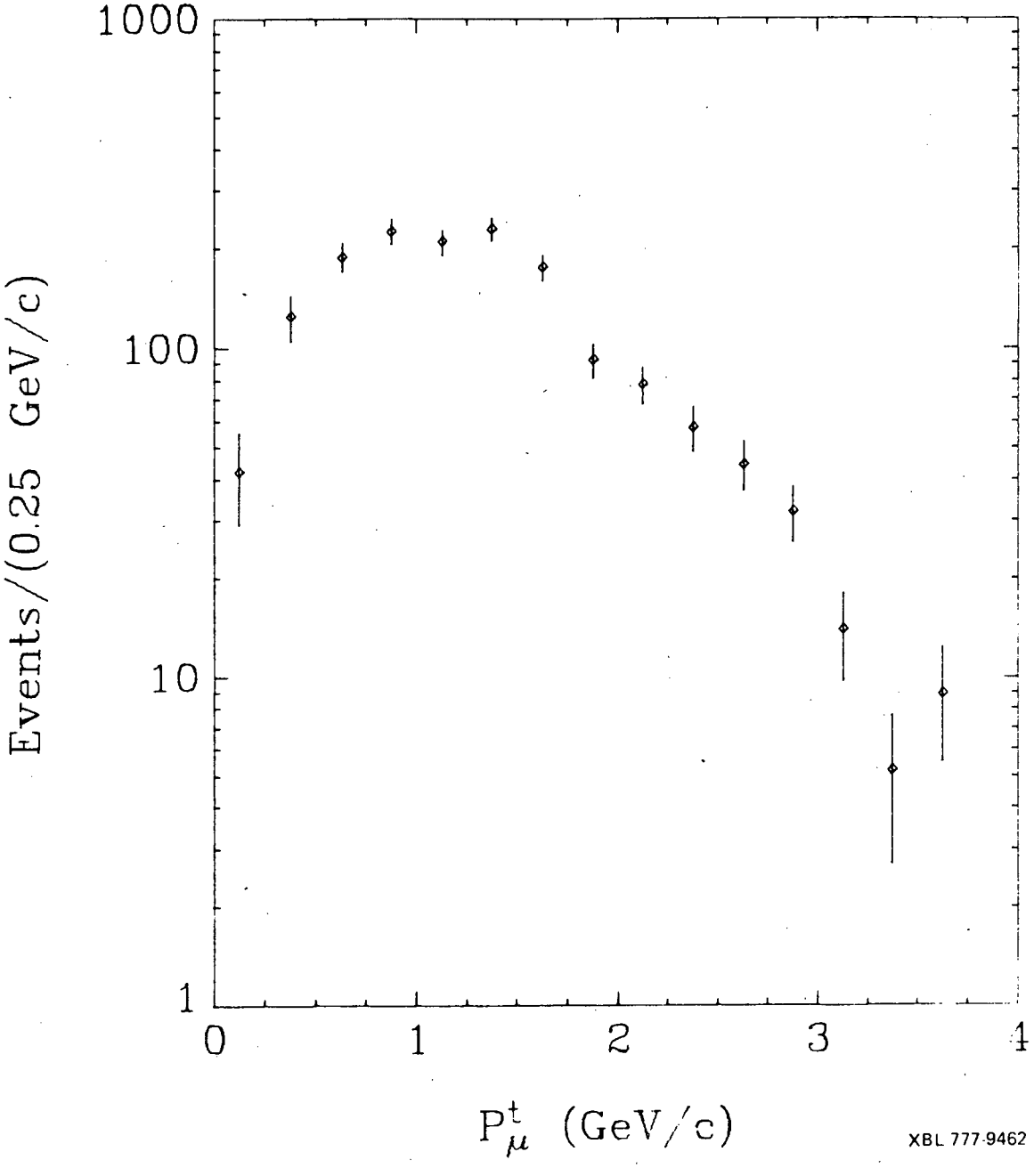

Figure 6

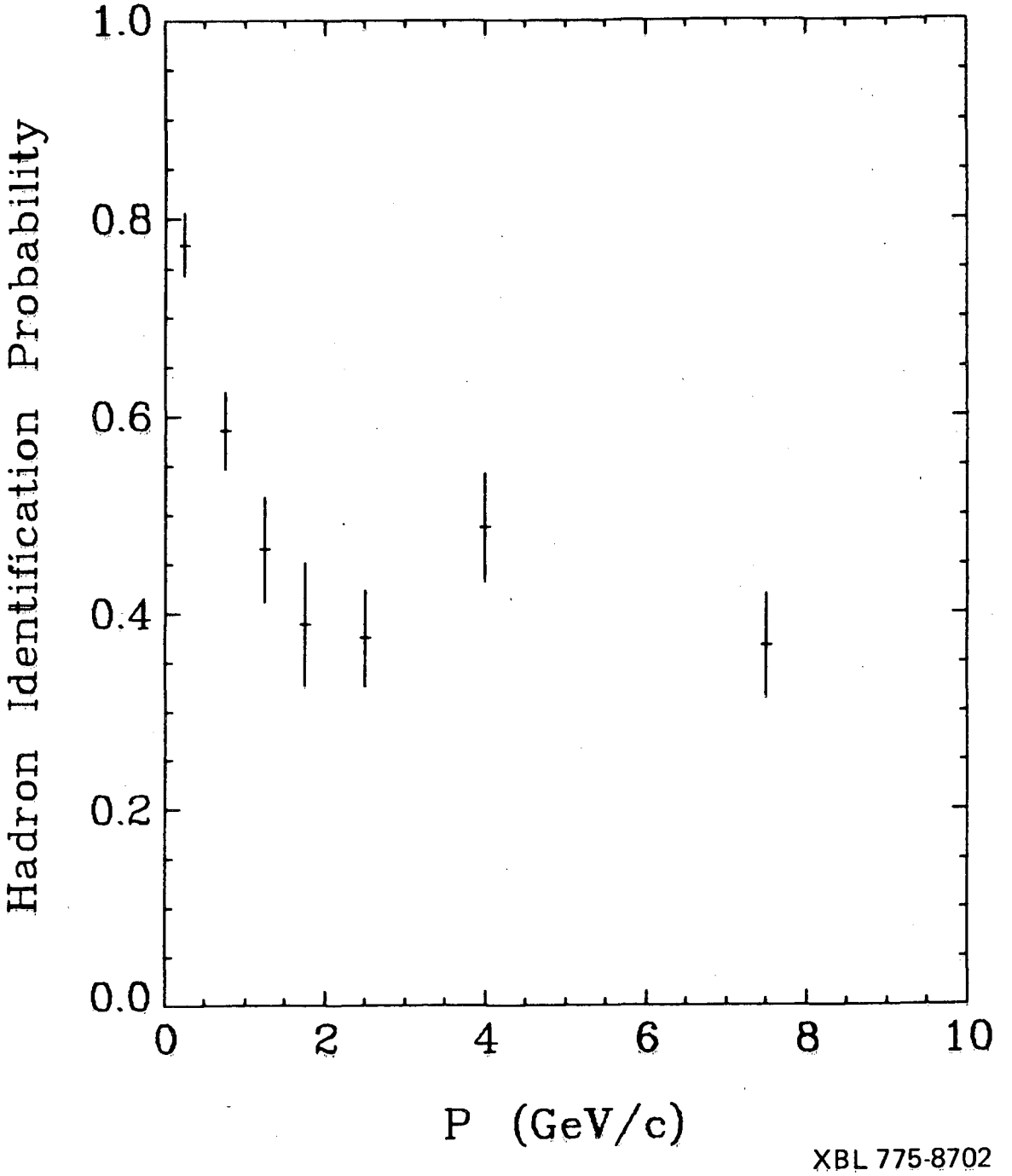
1.0
0.8
0.6
0.4
0.2
0.0
Hadron Identification Probability
0
2
4
6
8
10
P (GeV/c)
XBL 775-8702

Figure 7

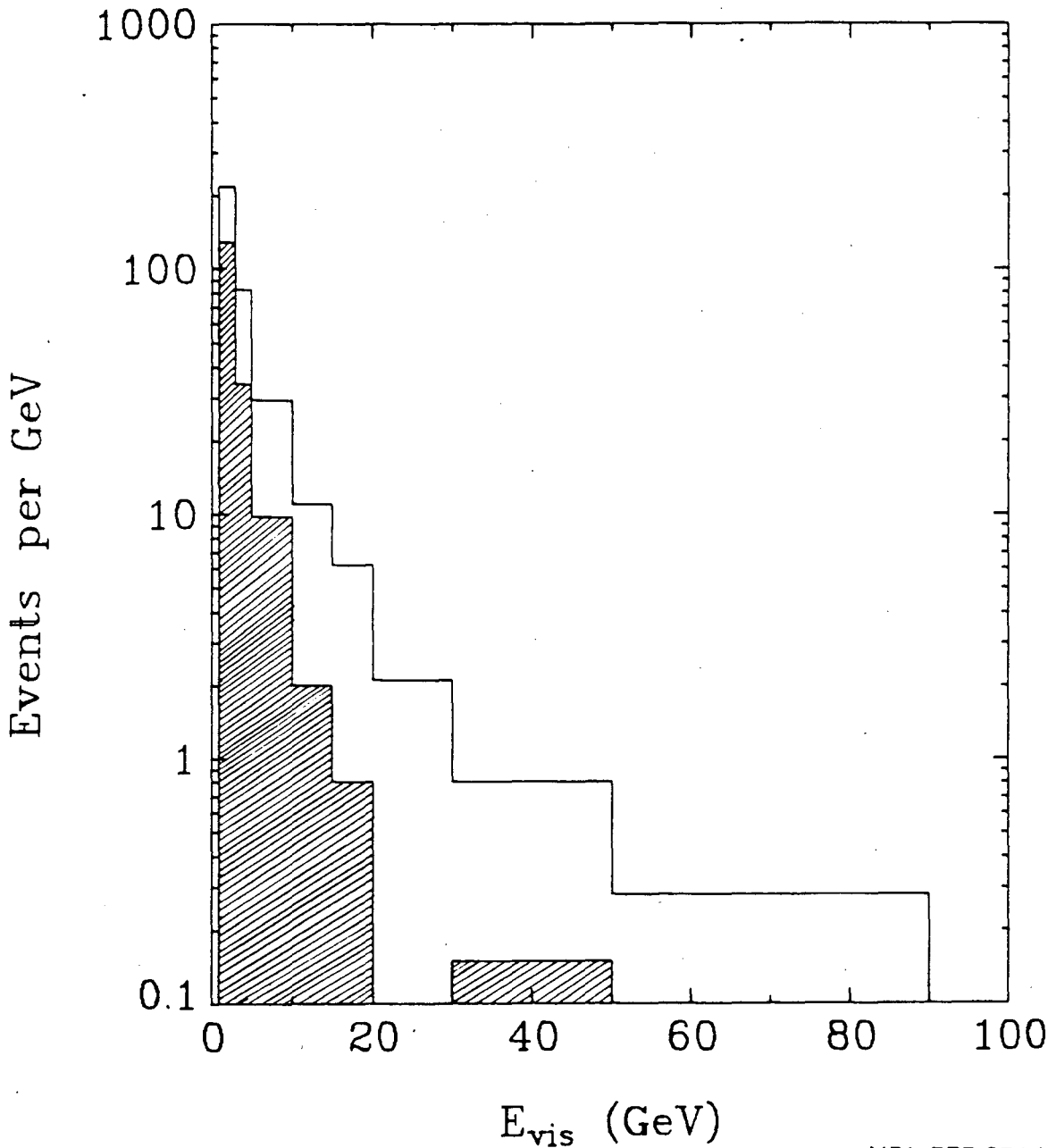

XBL 775-8714

Figure 8

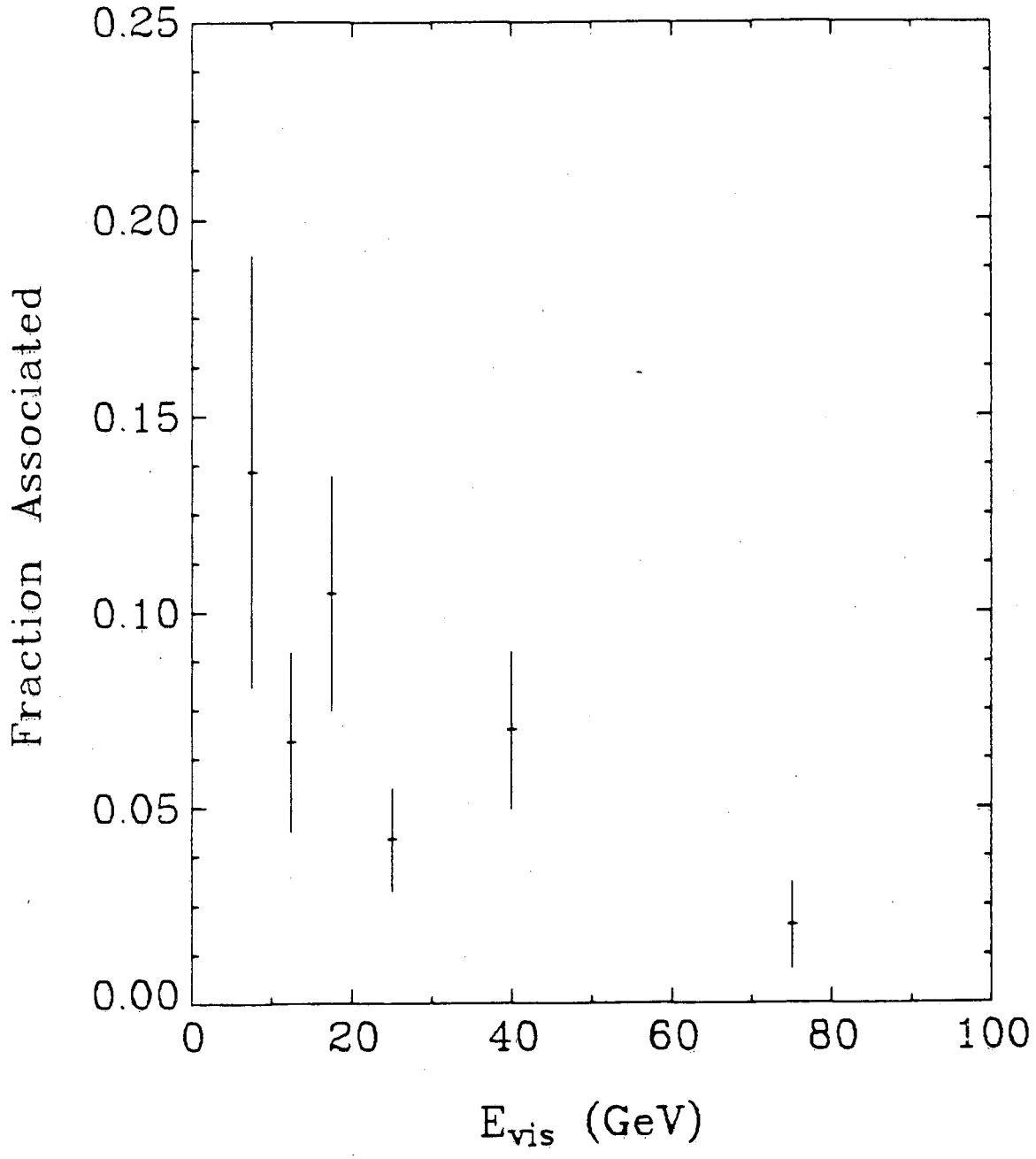

XBL 776-9033

Figure 9

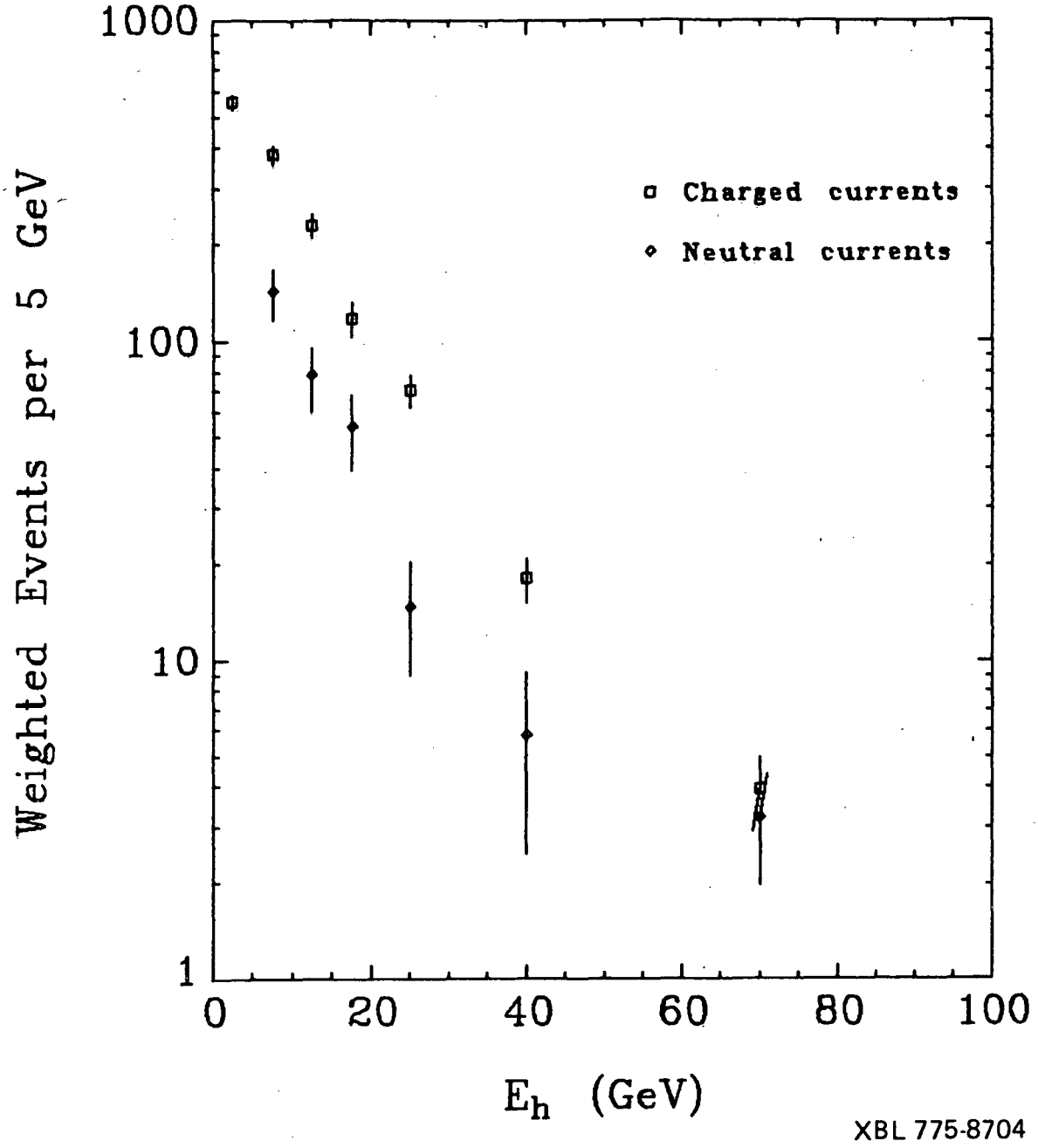
1000
100
10
1
0
20
40
60
80
100
Weighted Events per 5 GeV
E_h (GeV)
Charged currents
Neutral currents
XBL 775-8704

Figure 10

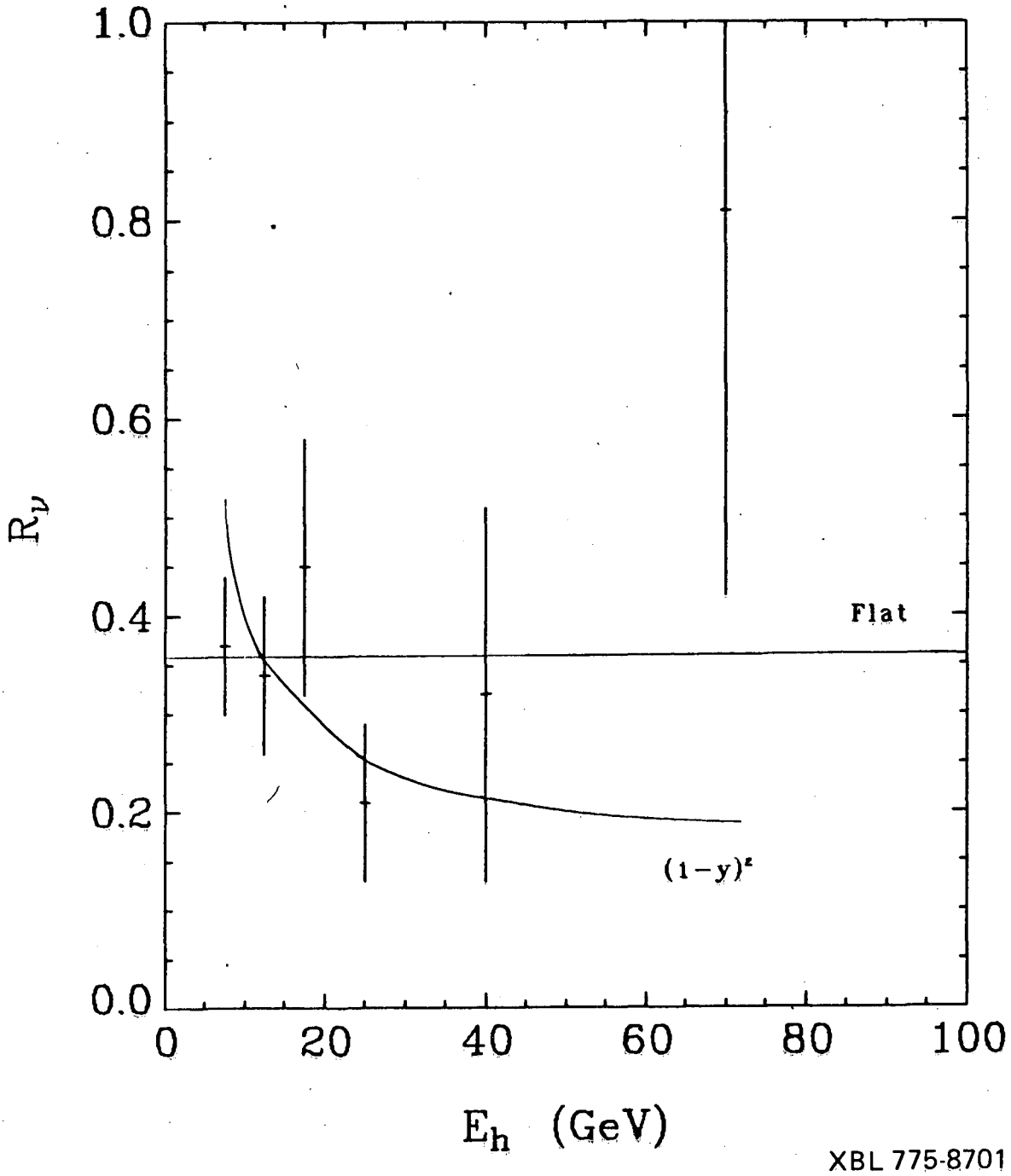

XBL 775-8701

Figure 11

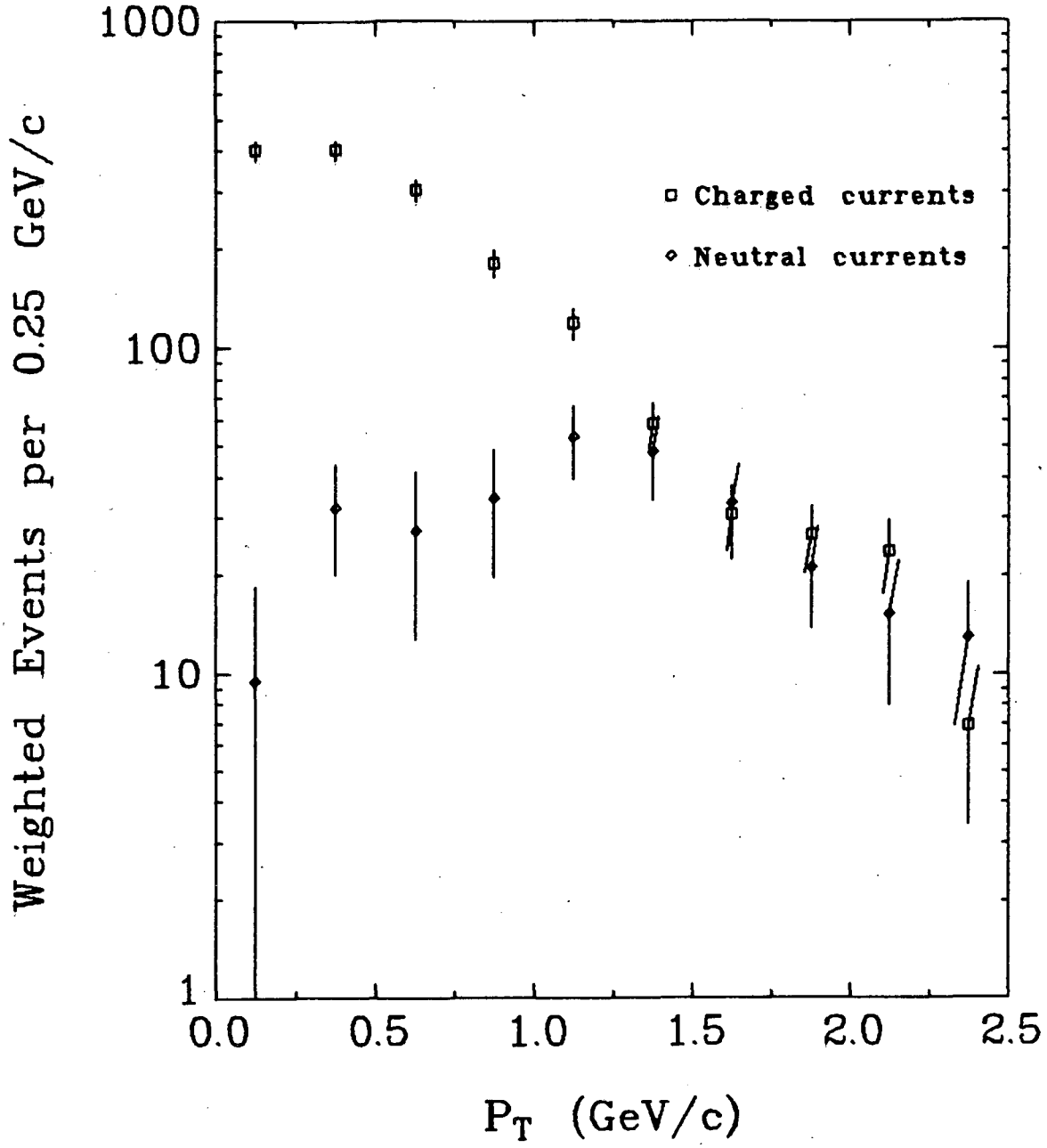

XBL 775-8709

Figure 12

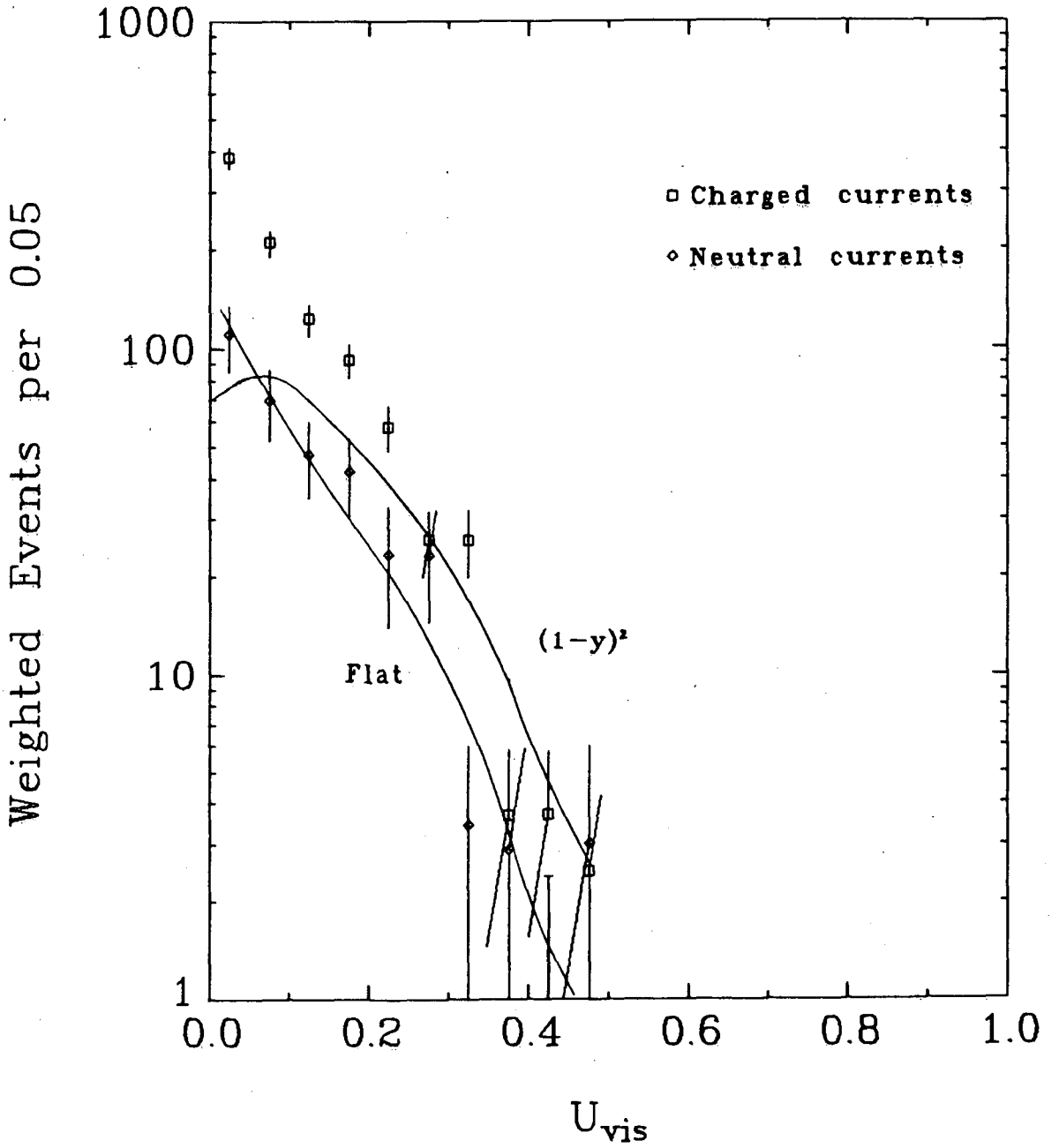

XBL 775-8711

Figure 13

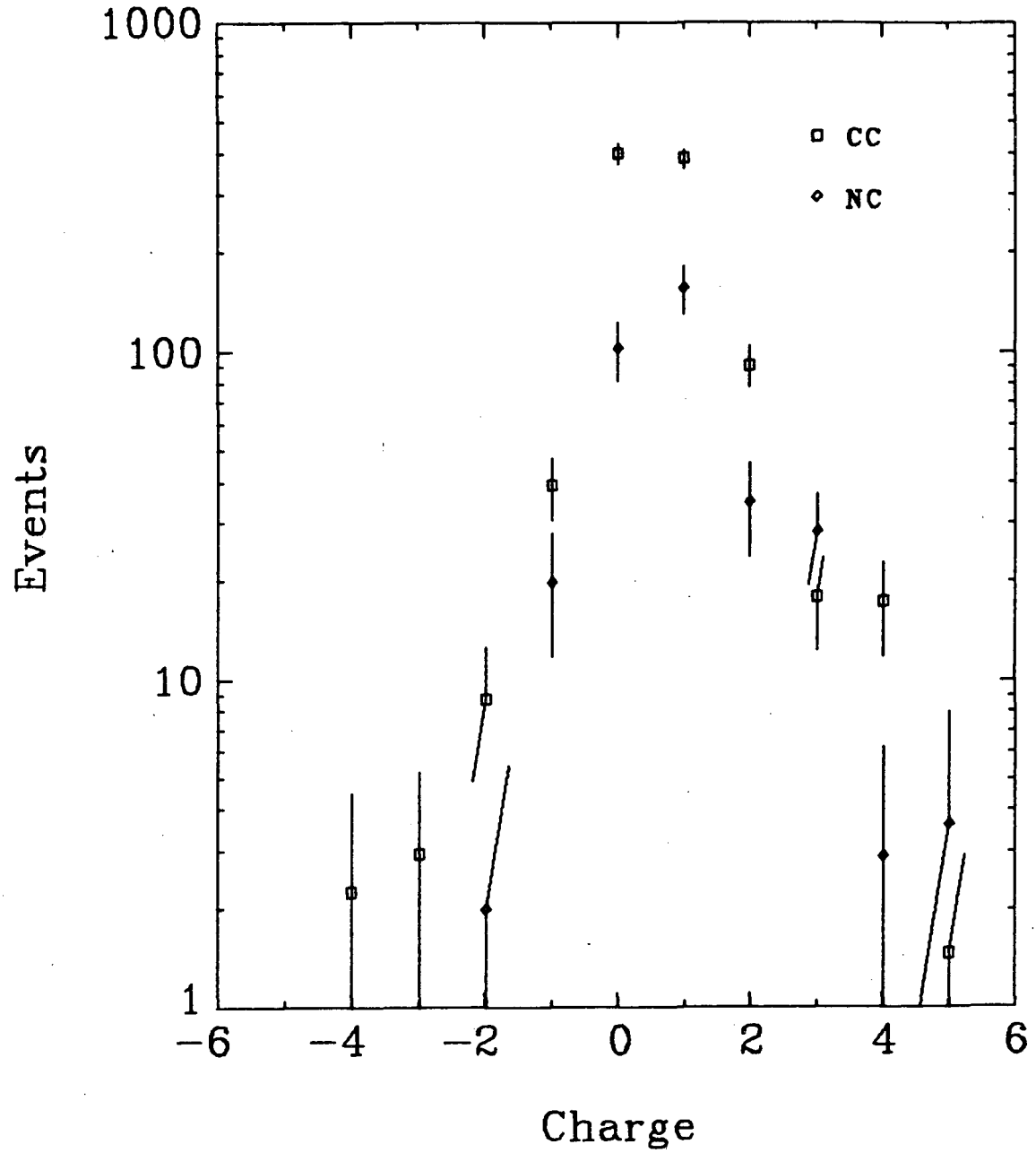

XBL 775-8707

Figure 14

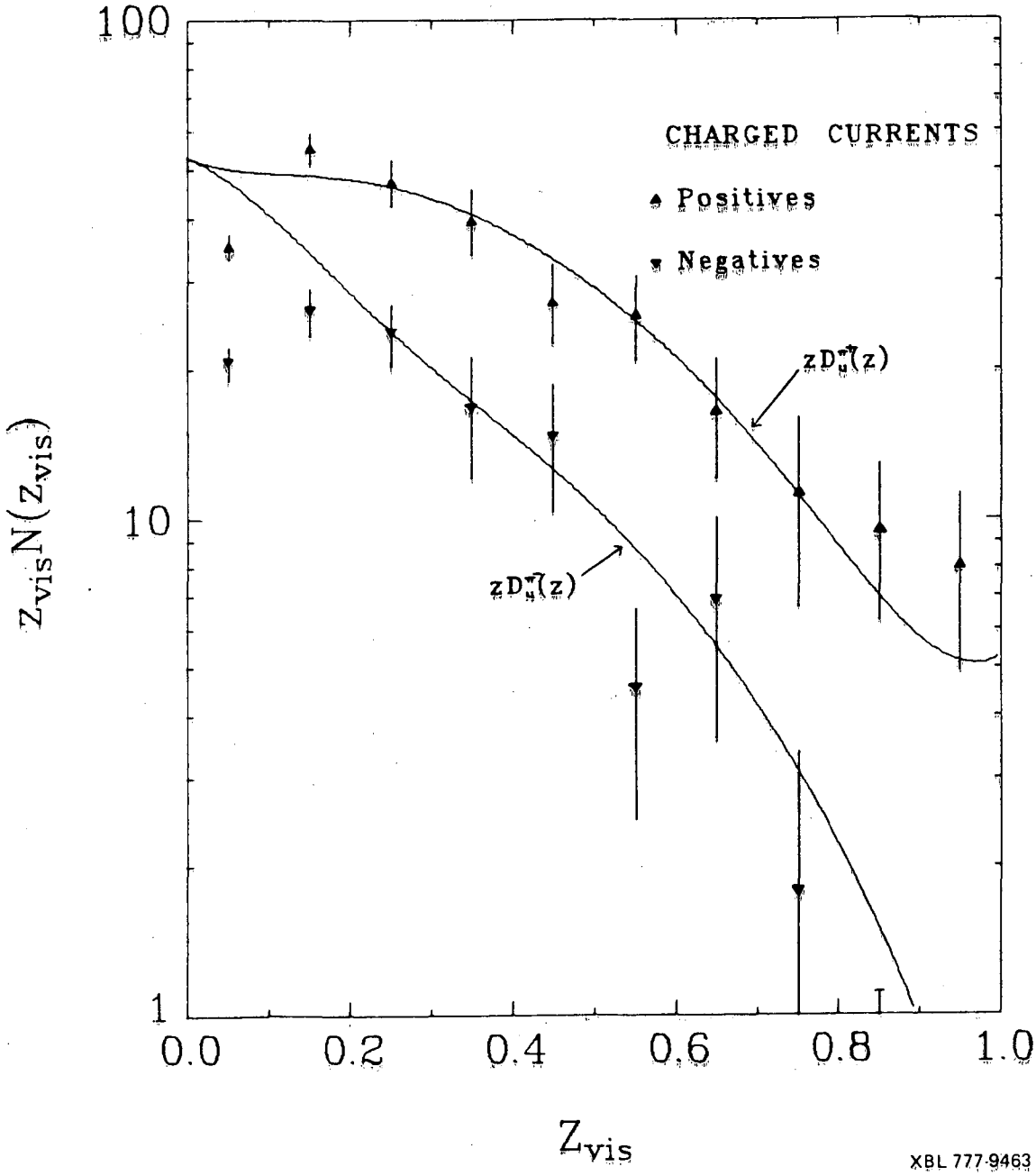

XBL 777-9463

Figure 15

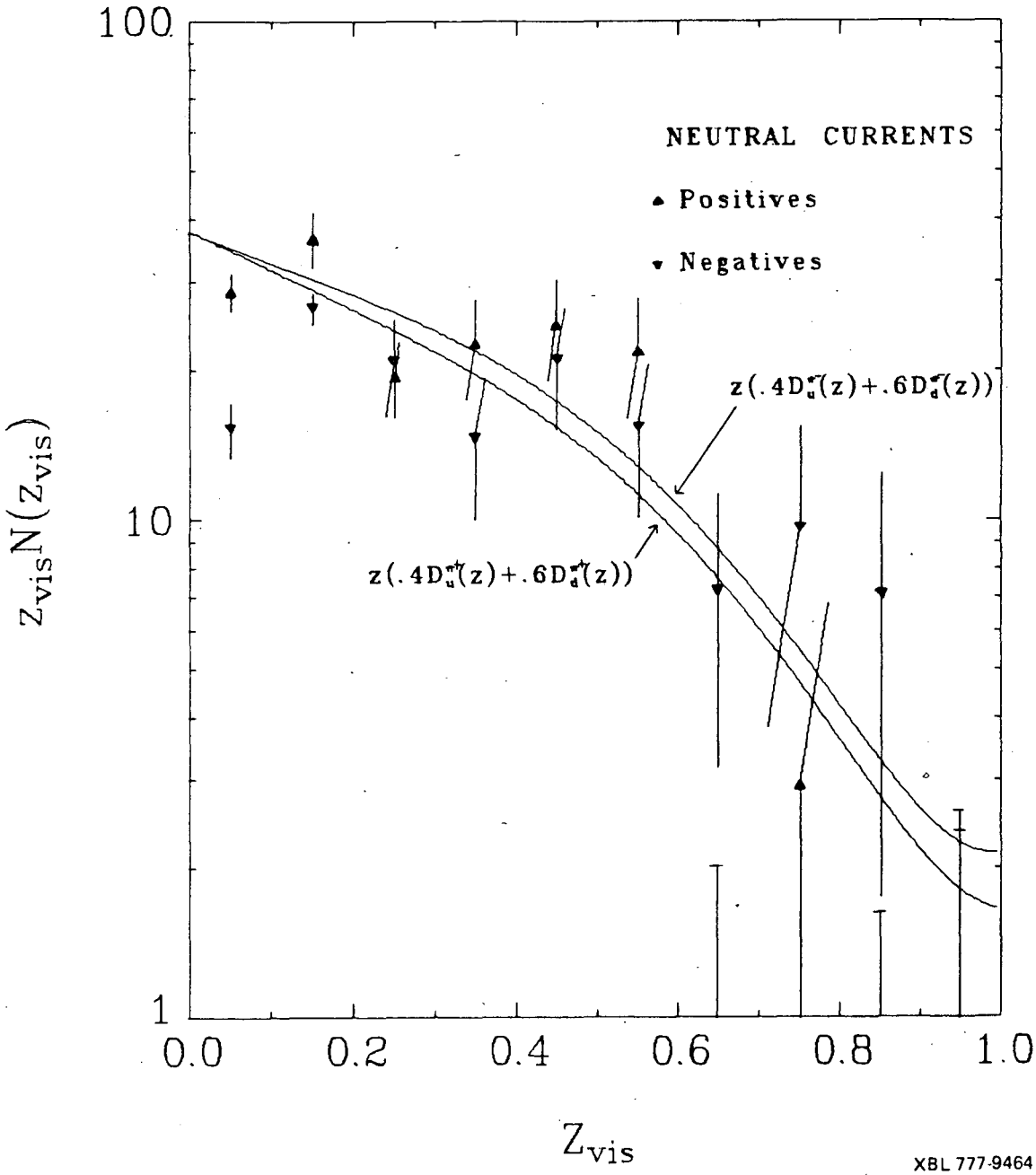
NEUTRAL CURRENTS
Positives
Negatives
z(.4D_u^π(z)+.6D_d^π(z))
z(.4D_u^π(z)+.6D_d^π(z))
100
10
1
0.0
0.2
0.4
0.6
0.8
1.0
Z_vis N(Z_vis)
Z_vis
XBL 777-9464

Figure 16

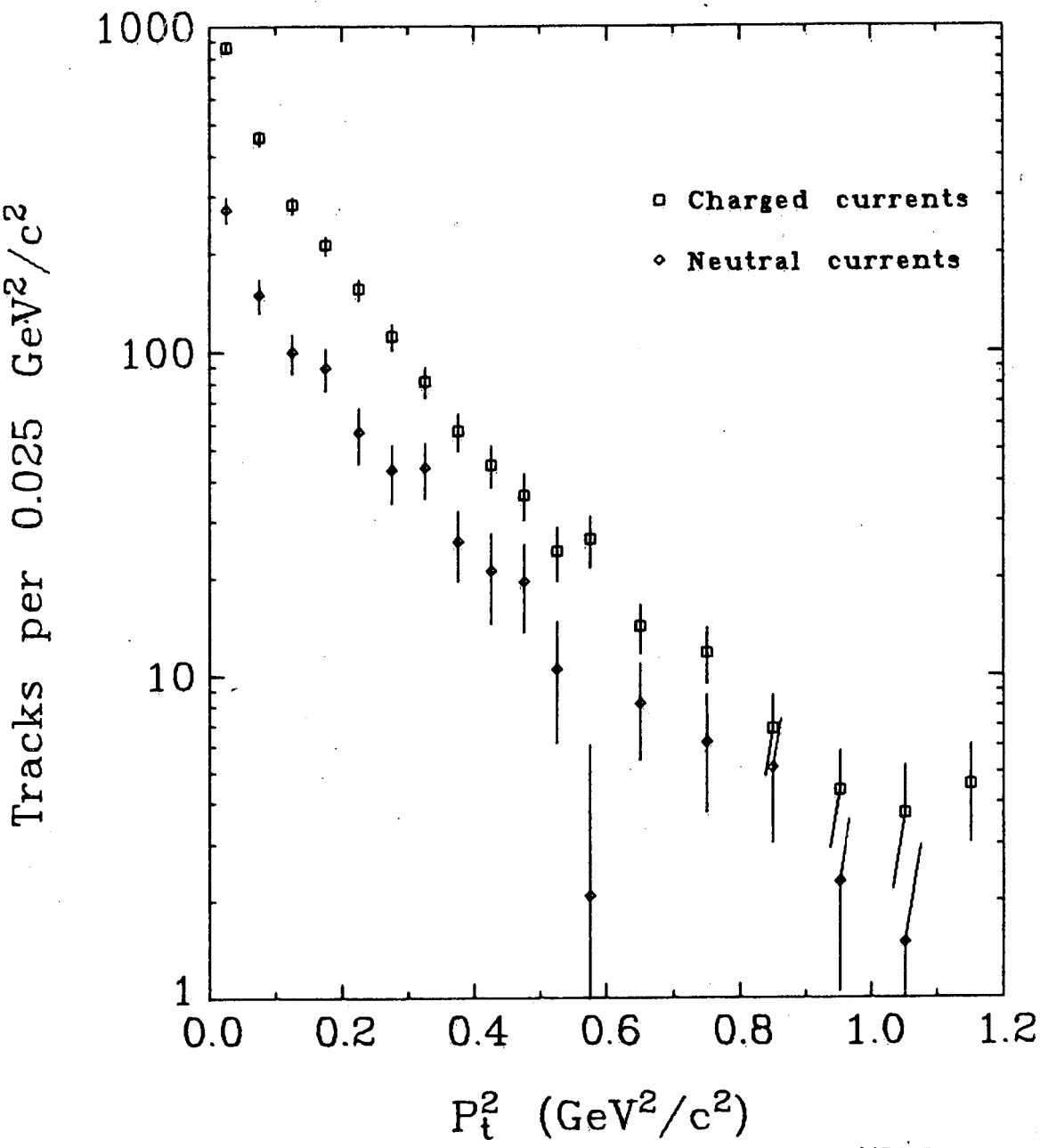

XBL 775-8712

Figure 17

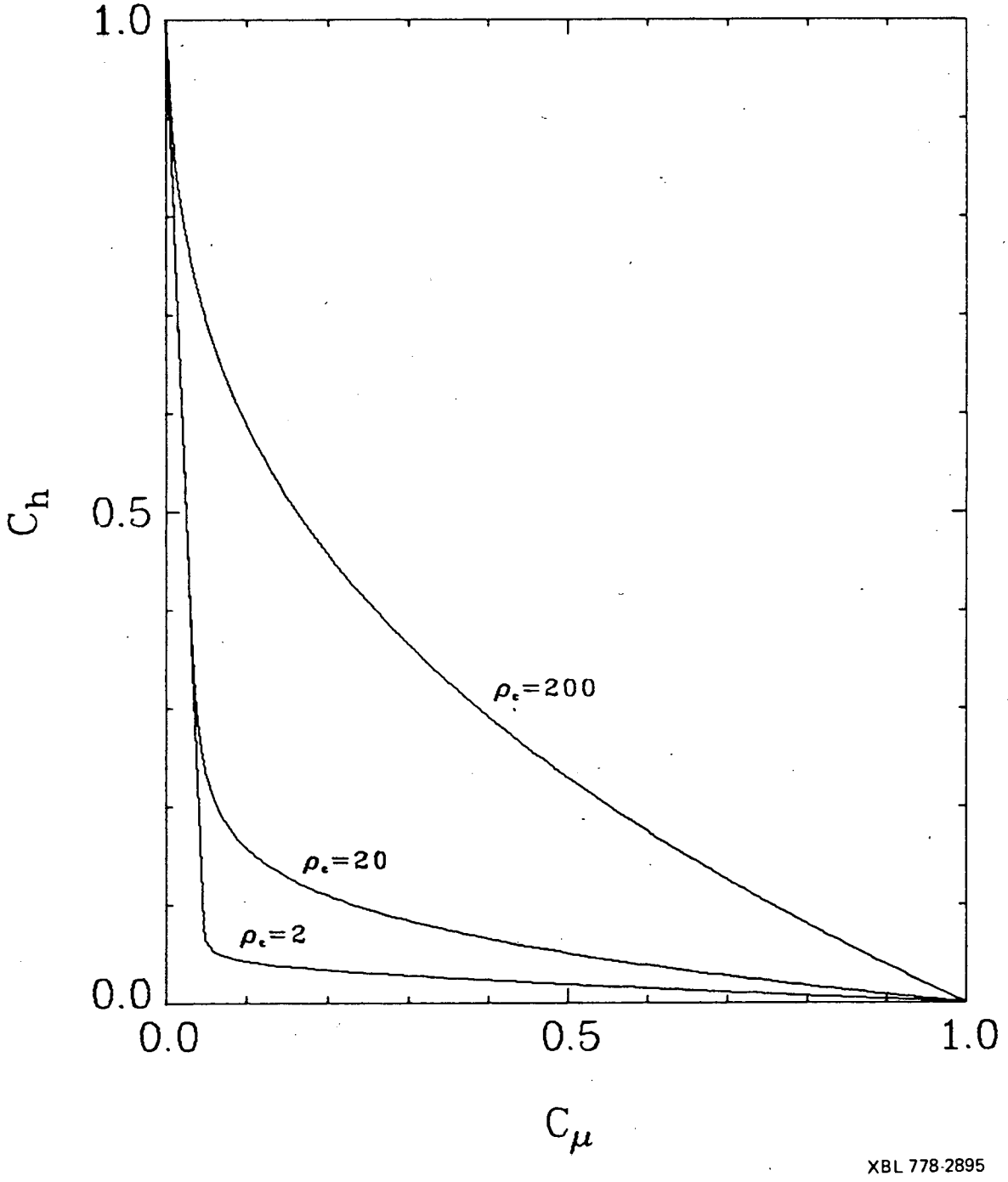

Figure 18

This report was done with support from the Department of Energy. Any conclusions or opinions expressed in this report represent solely those of the author(s) and not necessarily those of The Regents of the University of California, the Lawrence Berkeley Laboratory or the Department of Energy.

TECHNICAL INFORMATION DEPARTMENT
LAWRENCE BERKELEY LABORATORY
UNIVERSITY OF CALIFORNIA
BERKELEY, CALIFORNIA 94720